

New Young Brown Dwarfs in the Orion Molecular Cloud 2/3 Region¹

Dawn E. Peterson^{2,3,4}

Department of Astronomy, University of Virginia, Charlottesville, VA 22904

`dpeterson@cfa.harvard.edu`

S. T. Megeath^{2,3,5}

Harvard-Smithsonian Center for Astrophysics, 60 Garden Street, Cambridge, MA 02138

`megeath@physics.utoledo.edu`

K. L. Luhman

*Department of Physics and Astronomy, Pennsylvania State University, University Park,
PA 16802*

`kluhman@astro.psu.edu`

J. L. Pipher

Department of Physics and Astronomy, University of Rochester, Rochester, NY 14627

`jlipher@astro.pas.rochester.edu`

J. R. Stauffer

Spitzer Science Center, California Institute of Technology, MS 314-6, Pasadena, CA 91125

`stauffer@ipac.caltech.edu`

D. Barrado y Navascués

LAEFF-INTA, Apartado 50.727, E-28080 Madrid, Spain

`David.Barrado@laeff.esa.es`

J. C. Wilson

Department of Astronomy, University of Virginia, Charlottesville, VA 22904

`jcw6z@virginia.edu`

M. F. Skrutskie

Department of Astronomy, University of Virginia, Charlottesville, VA 22904

`mfs4n@virginia.edu`

M. J. Nelson

Department of Astronomy, University of Virginia, Charlottesville, VA 22904

`mjn4n@virginia.edu`

and

J. D. Smith

Steward Observatory, 933 N. Cherry Ave., Tucson, AZ 85721

`jdsmith@as.arizona.edu`

¹Some of the observations presented here were obtained at the MMT Observatory, Whipple Observatory, W.M. Keck Observatory, Las Campanas Observatory, Mount Graham International Observatory, and Apache Point Observatory. The MMT Observatory is a joint facility of the Smithsonian Institution and the University of Arizona. The W.M. Keck Observatory is operated as a scientific partnership among the California Institute of Technology, the University of California and the National Aeronautics and Space Administration. The W.M. Keck Observatory was made possible by the generous financial support of the W.M. Keck Foundation. The Apache Point Observatory 3.5-meter telescope is owned and operated by the Astrophysical Research Consortium. In addition, this publication makes use of data products from the Two Micron All Sky Survey, which is a joint project of the University of Massachusetts and the Infrared Processing and Analysis Center/California Institute of Technology, funded by the National Aeronautics and Space Administration and the National Science Foundation.

²Visiting Astronomer, Kitt Peak National Observatory, National Optical Astronomy Observatory, which is operated by the Association of Universities for Research in Astronomy, Inc. (AURA) under cooperative agreement with the National Science Foundation.

³Visiting Astronomer at the Infrared Telescope Facility, which is operated by the University of Hawaii under Cooperative Agreement no. NCC 5-538 with the National Aeronautics and Space Administration, Science Mission Directorate, Planetary Astronomy Program.

⁴Present address: Harvard-Smithsonian Center for Astrophysics, 60 Garden Street, Cambridge, MA 02138.

⁵Present address: Department of Physics and Astronomy, University of Toledo, Toledo, OH 43606.

ABSTRACT

Forty new low mass members with spectral types ranging from M4–M9 have been confirmed in the Orion Molecular Cloud 2/3 region. Through deep, I –, z' –, J –, H – and K –band photometry of a $20' \times 20'$ field in OMC 2/3, we selected brown dwarf candidates for follow-up spectroscopy. Low resolution far-red and near-infrared spectra were obtained for the candidates, and 19 young brown dwarfs in the OMC 2/3 region are confirmed. They exhibit spectral types of M6.5–M9, corresponding to approximate masses of 0.075–0.015 M_{\odot} using the evolutionary models of Baraffe et al. (1998). At least one of these *bona fide* young brown dwarfs has strong $H\alpha$ emission, indicating that it is actively accreting. In addition, we confirm 21 new low mass members with spectral types of M4–M6, corresponding to approximate masses of 0.35–0.10 M_{\odot} in OMC 2/3. By comparing pre-main sequence tracks to the positions of the members in the H-R diagram, we find that most of the brown dwarfs are less than 1 Myr, but find a number of low mass stars with inferred ages greater than 3 Myr. The discrepancy in the stellar and substellar ages is due to our selection of only low luminosity sources; however, the presence of such objects implies the presence of an age spread in the OMC 2/3 region. We discuss possible reasons for this apparent age spread.

Subject headings: infrared: stars – open clusters and associations: individual (Orion Molecular Clouds 2 and 3, OMC 2/3) – stars: formation – stars: imaging – stars: low-mass, brown dwarfs – techniques: spectroscopic

1. Introduction

The highly active star forming region known as the Orion Molecular Cloud 2/3 region (hereafter, OMC 2/3) is located in a molecular filament (Bally et al. 1987) in the northernmost part of the Orion A molecular cloud at a distance of 450 pc (Genzel & Stutzki 1989). This region contains one of the richest concentrations of protostars and prestellar cores known. Thirty-four submillimeter sources have been detected in OMC 2/3 at 1300 μm and 350 μm , evidence that it is a site of vigorous star formation activity (Chini et al. 1997; Lis et al. 1998). All six condensations in OMC 3, the northernmost part of OMC 2/3, fit the definition of Class 0 object, $L_{bol}/L_{submm} < 200$, and thus are in the earliest stages of stellar evolution (Chini et al. 1997). In addition, at least 80 knots of $\text{H}_2 v = 1 - 0 S(1)$ emission, signifying jets and outflows, have been detected in OMC 2/3, confirming the region’s extreme youth (Yu, Bally, & Devine 1997).

Although OMC 2/3 has such a high density of star-forming cores, as shown by the richness of submillimeter sources, the population of pre-main sequence (PMS) stars and young brown dwarfs has not been studied as extensively or to similar depth in the infrared as the Orion Nebula Cluster (ONC), which is directly south of OMC 2/3 (e.g. Slesnick, Hillenbrand, & Carpenter 2004; Lucas et al. 2001). As part of a study to survey the PMS star population in OMC 2/3, we present the results of a survey of young brown dwarfs. With the existence of brown dwarfs firmly established, attention has shifted towards understanding the formation mechanism. Reipurth & Clarke (2001) proposed that brown dwarfs are formed by the ejection of accreting “stellar embryos” from dynamically unstable systems of protostars, resulting in the premature termination of accretion and substellar masses. Our study of brown dwarfs in OMC 2/3 was initially motivated by this proposal; the detection of a large number of brown dwarfs around Class 0 sources would be evidence for ejection at slow velocities. Reipurth & Clarke (2001) suggest that given the amount of star formation activity, this would be the best place to find both very young brown dwarfs and potentially proto-brown dwarfs, and hence test models of their formation. A more detailed discussion of brown dwarf formation in OMC 2/3 will be discussed in a subsequent paper on *Spitzer* colors of the confirmed young brown dwarfs presented in this paper.

In order to obtain a complete census of the young brown dwarfs in OMC 2/3 (and eventually determine whether they are likely to have circumstellar disks), near-infrared observations are critical for identification. We performed near-infrared observations that are two to three magnitudes deeper than the Two Micron All Sky Survey (2MASS; Skrutskie et al. 2006) in order to identify the most deeply embedded substellar objects in OMC 2/3, down to $25 M_{Jup}$, based on 1 Myr isochrones (Baraffe et al. 1998). Before 2MASS, near-infrared observations of OMC 2/3 reached K -band magnitudes of 12.20 magnitudes (Johnson et al. 1990); as a comparison, for our near-infrared observations we reach a magnitude limit of $K = 17.9$.

Near-infrared and visible wavelength imaging and spectroscopy provide the information necessary for the selection and confirmation of substellar objects in star-forming regions. Young brown dwarfs, with ages much less than 10 Myr, are much more luminous and thus easier to detect than field brown dwarfs (typically older than 1 Gyr) at distances greater than 100 pc. However, the near-infrared colors of young brown dwarfs are similar to those of very low mass stars making it difficult to identify brown dwarfs from near-infrared photometry alone. Therefore techniques developed by Luhman (2000) are applied to select brown dwarf candidates in OMC 2/3 from combined, deep near-infrared and visible wavelength photometry. Once candidate brown dwarfs are photometrically selected, far-red ($0.6\text{--}1.0 \mu\text{m}$) and near-infrared ($0.8\text{--}2.5 \mu\text{m}$) spectroscopic observations are used to confirm the candidates as *bona fide* brown dwarfs.

We present a multiwavelength analysis of the OMC 2/3 region to identify the population of young brown dwarfs. In Section 2, we introduce the ground-based imaging of the OMC 2/3 region. Next, in Section 3, we describe the techniques used for selecting candidate young brown dwarfs for spectroscopy using the multiwavelength photometry. Then, we describe the spectroscopic observations (Section 4) and the spectral type classification methods used as well as the spectral types determined from the spectra (Section 5). Finally, we discuss the age of OMC 2/3 in Section 6.

2. Observations: Imaging

2.1. Near-Infrared Imaging

The near-infrared observations of OMC 2/3 were obtained with SQIID (Ellis et al. 1992), the Simultaneous Quad Infrared Imaging Device on the 2.1-meter telescope at Kitt Peak National Observatory during the period of 2000 December 11–13. The conditions were non-photometric, with thin clouds, and the seeing was around $2''$ (closer to $1.8''$ in K -band). SQIID utilizes a 1024×1024 InSb detector array with independent 512×512 quadrants that are filtered at Barr J ($1.27 \mu\text{m}$), Barr H ($1.67 \mu\text{m}$), Barr K ($2.22 \mu\text{m}$) and Barr PAH ($3.30 \mu\text{m}$). As seen in Figure 1, our SQIID image mosaic toward OMC 2/3 totals a $20' \times 20'$ field of view centered slightly north of OMC 2, $\alpha = 05^h 35^m 22.8^s$, $\delta = -05^\circ 6' 37.1''$ (J2000), at J , H and K (no useful data were obtained at $3.30 \mu\text{m}$ with SQIID). These wide-field mosaics were obtained by mapping the region in a 4×4 grid with approximately $90''$ of overlap between images in adjacent grid positions. Each image in the grid has 512×512 pixels; with a platescale of $0.69''/\text{pixel}$, the total size of the final mosaic is $20' \times 20'$. The 4×4 map was repeated seven times with slightly offset positions each time; the typical total integration time for each image is 7 minutes.

Customized Interactive Data Language (IDL) programs were implemented to perform the image reduction including linearity, flat fielding, background subtraction, the elimination of bad pixels, and distortion correction, as well as creation of individual mosaics and aperture photometry. Calibration of the SQIID observations was done by comparison with 2MASS photometry; thin clouds were present during the observations, and thus the data were not calibrated with standard stars. To properly compare the 2MASS stellar magnitudes with the magnitudes of the sources in our SQIID images, 15–30 stars were chosen for calibration in each of the sixteen fields. Stars which were determined by Carpenter, Hillenbrand, & Skrutskie (2001) to show variability were not among those included for calibration. In addition, sources brighter than the saturation limits of $J = 10.31$, $H = 10.06$ and $K = 9.45$ as well as sources fainter than the 2MASS completeness limits

were not included. Each 512×512 pixel frame was calibrated individually by finding the offset between the instrumental magnitudes derived in that frame and the magnitudes from the 2MASS Point Source Catalog for each selected source. The rms scatter of the residuals between the 2MASS and SQIID data sets ranges from 0.05 to 0.08 magnitudes; this is on the order of the typical uncertainty in the instrumental magnitude for SQIID (for which the maximum allowed was 0.15 magnitudes). After the calibrated frames were combined into mosaics, we compared the photometry from our calibrated SQIID mosaics with 2MASS to look for systematic offsets between the two systems (mainly due to the difference in the K bandpasses) and found the following relations:

$$J_{2MASS} - J_{SQIID} = -0.0039(\pm 0.0026)(J - K)_{SQIID} - 0.014(\pm 0.004) \quad (1)$$

$$H_{2MASS} - H_{SQIID} = -0.026(\pm 0.002)(J - K)_{SQIID} + 0.020(\pm 0.004) \quad (2)$$

$$K_{2MASS} - K_{SQIID} = 0.017(\pm 0.001)(J - K)_{SQIID} - 0.023(\pm 0.002) \quad (3)$$

where K_{2MASS} is a K_S filter. Over 350 stars in each band were used to calculate these relationships; all have photometric uncertainties less than 0.10 magnitudes.

Once the images were calibrated, IDL routines including PhotVis, a graphical interface for the IDL aperture photometry routine (Gutermuth et al. 2004), were used to perform aperture photometry on the final image mosaics. A synthetic aperture radius of 3 pixels was used with a small sky annulus of 2 pixels in width (identical to that used for calibration). The final source list contained 823 sources that appeared in all three bands with photometric uncertainties less than 0.15 magnitudes; only sources with J -, H - and K -band photometric uncertainties less than 0.15 magnitudes were used for analysis. Note that the photometric uncertainties tabulated throughout this paper do not take into account the uncertainties in the absolute calibration discussed in the previous paragraph. The tabulated uncertainties are calculated (by PhotVis) from the expected shot noise and read noise and the measured RMS variations in the background annulus.

The limiting magnitudes reached with the detection criteria were $J = 19.4$, $H = 18.3$ and $K = 17.9$. We derived 90% completeness limits by adding synthetic stars to our images for a range of magnitudes using a Gaussian PSF with the same FWHM as that of our images and performing the same point source extraction. Measurements were rejected if they had photometric uncertainties greater than 0.15 magnitudes and if the recovered magnitude was more than 3σ brighter than the input magnitude, indicating that a star was likely coincident with a synthetic star. Table 1 lists the magnitude at which 90% of the stars were recovered for the J -, H - and K -bands. For comparison, published completeness limits for 2MASS

are $J = 15.8$, $H = 15.1$ and $K_s = 14.3$ magnitudes (where source counts are $> 99\%$ complete at the $S/N=10$ limits; Skrutskie et al. 2006).

2.2. I - and z' -Band Imaging

The visible wavelength I - and z' -band images were obtained under photometric conditions with $\sim 2.5''$ seeing, 2002 December 7 using the 4-Shooter camera on the 1.2-meter telescope at Fred Lawrence Whipple Observatory (FLWO). The 4-Shooter camera has four 2048×2048 arrays, arranged in a 2×2 grid with $45''$ separation between chips. The images were binned 2×2 during readout, resulting in a pixel scale of $0.67''/\text{pixel}$. The final $20' \times 20'$ field was centered to match the SQUID J -, H - and K -band images. OMC 2/3 was imaged at Harris I (8100 \AA) and z' (9100 \AA), twice at each band with an integration time of 20 minutes each, for a total of 40 minutes at each wavelength. Similar steps were taken to reduce the I - and z' -band images as for the SQUID J -, H - and K -band images, including bias subtraction, flat fielding, the elimination of bad pixels, and distortion correction.

The standard stars used to calibrate the 4-Shooter images of OMC 2/3 are from the Landolt (1992) SA98-670 and SA98-618 fields. The I -band data were calibrated from standards in the Cousins I system without including a color dependence term because the I -band filter at FLWO is similar. Since z' magnitudes are not tabulated in Landolt (1992), the z' magnitudes were estimated from the I -band magnitudes of standard stars with neutral colors. The stars in the Landolt (1992) fields with $R - I$ colors less than 0.4 were used, and $I - z' = 0$ assumed. Using this calibration for our z' magnitudes is sufficient because these data are only used to identify young low mass candidates from background sources.

Each standard field was imaged twice over the course of the night so that an airmass correction could be accounted for in the calibration. Aperture photometry was obtained using a radius of 6 pixels with a sky annulus of 4 pixels in width for both the standard stars used for calibration and for the OMC 2/3 sources. The rms scatter of the residuals for the Landolt (1992) standard stars imaged with the 4-Shooter is less than 0.05 magnitudes; this calibration uncertainty is on the order of the typical intrinsic photometric uncertainties for the 4-Shooter observations. Only sources with photometric uncertainties less than 0.15 magnitudes were used in our analysis (as with the J -, H - and K -band data, calibration uncertainties are not included in the tabulated uncertainties). Completeness limits for I - and z' -band were analyzed in the same way as for the J -, H - and K -band data (see Section 2.1) and are also listed in Table 1. The completeness limits for the visible wavelength photometry were difficult to assess because of nebulosity from the ONC in the southern part of the image. Therefore the 90% completeness limits quoted in Table 1 are for the region

north of a declination of -5.15 ; if we include the entire image in our analysis, the magnitudes quoted in Table 1 are 80% complete.

3. Photometric Selection of Brown Dwarf Candidates

Candidate young brown dwarfs in OMC 2/3 are selected from the merged SQUID and 4-Shooter I –, J –, H – and K –band photometry. Brown dwarfs are identified by two criteria: their low luminosity and, when they are detected in the I –band, their red colors. These candidates still require confirmation with spectroscopic observations, though, to eliminate contamination from faint background stars and to distinguish between older low mass stars both in OMC 2/3 and in the foreground. The candidates are selected for follow-up spectroscopy in the far-red, and in cases where they are too faint to detect in the I –band, in the near-infrared.

To search for brown dwarfs on the basis of their low luminosities, candidates are initially selected from their positions on an H versus $J-H$ color-magnitude diagram (CMD), as shown in Figure 2. The models of Chabrier & Baraffe (1997) show that the hydrogen burning limit (HBL) for solar metallicity objects is at $0.075 M_{\odot}$. However, given the uncertainty in the ages of the sources, we consider a “soft boundary” of $0.080 M_{\odot}$ to be used to guide the selection of objects and not as the precise location of the HBL. To find the corresponding luminosity, an age and distance must be adopted and we adopt a distance of 450 pc and an age of 1 Myr. Several recent studies of the distance to Orion place the distance closer, consistent with a value of 420 pc (Hirota et al. 2007; Jeffries 2007a; Menten et al. 2007; Sandstrom et al. 2007). Since this result was published after our analysis, we use 450 pc throughout this paper. Uncertainties that arise from this are discussed in Section 6.1. Adopting an age of 1 Myr is motivated by both the concentration of young protostellar objects in this region and the age of the neighboring ONC ($< 1-2$ Myr; Hillenbrand (1997)). Using the 1 Myr evolutionary tracks of Baraffe et al. (1998) and the spectral type versus effective temperature scale from Luhman et al. (2003), the spectral type corresponding to a mass of $0.080 M_{\odot}$ is approximately M6–M6.5; in this paper, we use M6.5 as the fiducial boundary between stellar and substellar objects.

At the faint magnitudes typical of young brown dwarfs, contamination by background stars is considerable. Studies of the Taurus and IC 348 young clusters (Luhman 2000, 1999) have shown that members of a young population can be separated from background stars using visible and near-infrared wavelength CMDs (e.g. H versus $I-K$). As Luhman (2000) showed with the Taurus region, background stars follow a different locus than cluster members. Therefore the Luhman (2000) techniques of using combined, deep near-infrared

and visible wavelength photometry to select brown dwarf candidates for spectral observations are used here for OMC 2/3.

For the candidate selection, we first placed all the sources detected at I –, J –, H – and K –band that fell below the $0.080 M_{\odot}$ reddening vector in the H versus $J - H$ CMD (Figure 2) on a $I - K$ versus $J - H$ color-color diagram and a dereddened, H versus $I - K$ CMD. Figure 3 shows how the spectroscopically confirmed brown dwarfs in OMC 2/3 are located in a very limited region of a dereddened, H versus $I - K$ CMD, as was also seen in Taurus (Luhman 2000). We note that there are a few sources located in this region of the CMD with colors and magnitudes similar to the brown dwarfs which we have not obtained spectra of because they were too faint. For the initial candidate list, we selected sources with dereddened H –band magnitudes greater than 13 and with dereddened $I - K$ colors greater than or equal to 3. Although a $I - K$ versus $J - H$ color-color diagram and I versus $I - z'$ CMD are not shown here, they were also useful for candidate selection when comparing with reddening vectors for sources less massive than $0.080 M_{\odot}$. The dereddened $I - K$ color is used as a proxy for temperature for sources with I –band detections. The dereddening is performed using the extinction law of Cohen et al. (1981) and adopting a typical $(J - H)_0$ color of 0.6 (see Appendix A for a complete description). By identifying sources with $I - K$ colors consistent with young brown dwarfs ($I - K \geq 3$), as seen in Taurus, we reduce contamination both from faint background stars and from older low mass stars in OMC 2/3 and the foreground.

For highly extinguished sources (i.e. sources that did not have I –band, and in some cases, J –band detections), we rely on their dereddened luminosity and colors in the near-infrared alone, which makes it difficult to distinguish cool, substellar members from background stars: giants as well as older, higher temperature dwarfs along the line of sight. The candidate brown dwarfs selected for near-infrared spectroscopy were chosen because they met several criteria. First, their K –band magnitudes range from 13 to 16 magnitudes (where $K = 16$ is the magnitude limit reached with SpeX) and they fall below the $0.080 M_{\odot}$ reddening vector on the J versus $J - H$ CMD and/or K versus $H - K$ CMD (see Figure 4). In the CMD, brown dwarfs confirmed from far-red spectroscopy are denoted by filled squares (note that chronologically, the far-red spectra were obtained earlier, so brown dwarf status was already confirmed for some sources when the near-infrared candidates were selected and observed). Also, many of the candidate brown dwarfs selected for near-infrared spectroscopy were chosen because they exhibit $A_V > 7$. This criterion limits overlap with the optically visible sample and reduces contamination from foreground stars. Additionally, the sources with high S/N J –band magnitudes were placed on a near-infrared color-color diagram as seen in Figure 5 to reject sources with colors similar to those of giants (Bessell & Brett 1988, red dotted line in Figure 5).

4. Spectroscopic Observations

Spectra were obtained for a total of 88 brown dwarf candidates identified in OMC 2/3. This includes 32 candidates obtained with the MMT and Keck telescopes in the far-red spectral regions, and 56 highly extinguished candidates observed in the near-infrared regime with the Infrared Telescope Facility (IRTF).

4.1. Far-Red Spectroscopy

Far-red (0.6–1.0 μm) spectral observations were obtained for a total of 32 brown dwarf candidates in OMC 2/3 on four different occasions. Spectra of seven brown dwarf candidates were obtained 2002 November 5 with the Low Resolution Imaging Spectrograph (Oke et al. 1995) on the 10-meter Keck I telescope from about 6400 to 7700 \AA using the 1200 lines/mm grating; spectra were obtained with about a 2 \AA resolution. Spectra of twelve brown dwarf candidates were obtained on 2002 November 11 and 2002 December 15 using the Blue Channel Spectrograph on the MMT Observatory 6.5-meter telescope, centered at 7600 \AA using the 600 lines/mm grating. Lastly, spectra of thirteen brown dwarf candidates were obtained on 2003 January 26–27 with the Red Channel Spectrograph at the MMT, also centered at 7600 \AA using the 270 lines/mm grating.

In addition to the spectra of the candidates, arc (HeNeAr) lamp spectra were obtained for wavelength calibration and continuum “bright” lamps were observed for flat fielding. All of the far-red spectra are reduced similarly. First a bias frame is subtracted from the source frames, then they are flat fielded using the spectra of the bright lamps. Finally the source spectrum is extracted and wavelength calibrated using the HeNeAr lamp spectrum.

4.2. Near-Infrared Spectroscopy

4.2.1. *SpeX* Data

For the highly extinguished OMC 2/3 brown dwarf candidates, low resolution, near-infrared spectroscopy was obtained with the *SpeX* spectrograph at the Infrared Telescope Facility (IRTF) on Mauna Kea (Rayner et al. 2003). A total of 56 candidates were observed with *SpeX*, where four of them overlap with the aforementioned candidate spectra obtained in the far-red. Observations with *SpeX* were made in single-prism mode ($\lambda/\Delta\lambda \sim 250$) on the nights of 2003 December 21–23, 2005 January 5, and 2006 January 3–5. Near-infrared spectroscopy is the only reliable means for obtaining an accurate census of

the more heavily embedded (and therefore reddened) brown dwarfs in OMC 2/3 and the wavelength coverage of SpeX in the single-prism mode (0.8–2.5 μm) combined with the high, dry site of Mauna Kea is ideal for accurately measuring water absorption in young brown dwarfs. This is important because the spectral types of our OMC 2/3 brown dwarf candidates observed with SpeX are established from the depth of the water vapor absorption bands (Wilking, Greene, & Meyer 1999), as will be described in Section 5.

In addition to the 56 OMC 2/3 candidates that have been observed with SpeX to date, 23 optically classified standards have also been observed. These standards are young brown dwarfs and low mass stars (in OMC 2/3 and Taurus), field dwarfs, and giants (Briceño et al. 2002). These comparison spectra were obtained in order to quantify the shape of the water absorption features indicative of late M-type stars, and thus provide a set of spectral calibration templates.

The SpeX spectra obtained 2003 December 21–23 and 2005 January 5 were reduced using the Spextool package version 3.2 (Cushing, Vacca, & Rayner 2004) and those obtained 2006 January 3–5 were reduced using version 3.4. Several spectra from the 2003 observing run were re-reduced with version 3.4 for comparison; no difference was found. The Spextool package performs the basic reduction steps described in the previous section for the reduction of the far-red spectra. Observations of the nearby A0V star, HD 37887, were obtained between each source to facilitate the removal of telluric features. The Spextool package uses a high resolution model of Vega to remove the hydrogen absorption features in the stellar spectrum, as described by Vacca, Cushing, & Rayner (2003).

4.2.2. *CorMASS Data*

Six near-infrared spectra were obtained using CorMASS (where two of them overlap with candidate spectra obtained in the far-red). CorMASS, the Cornell Massachusetts Slit Spectrograph (Wilson et al. 2001), is a cross-dispersed spectrograph with a $\lambda/\Delta\lambda$ of approximately 300 and wavelength coverage of 0.75–2.5 μm , similar to SpeX. One object was observed 2005 May 1 at the 6.5-meter Magellan (Clay) Telescope at Las Campanas Observatory. Three objects were observed on the dates of 2004 October 23 and 2005 January 29 at the 1.8-m Vatican Advanced Technology Telescope at Mount Graham International Observatory. Two objects were observed on the dates of 2005 October 16 and 2006 January 18 at the Apache Point Observatory (APO) 3.5-meter telescope.

Data reduction was performed using Cormasstool, a modification of Spextool (Cushing, Vacca, & Rayner 2004), again including the basic reduction steps described in the previous sections. The stan-

ard A0V star (HD 37887) was used to remove the telluric features.

5. Spectral Classification

5.1. Far-Red Spectra

5.1.1. *Molecular Features*

Spectral types are determined by the relative strengths of specific atomic and molecular features. The wavelength range of the far-red spectra we obtained, 0.6–1.0 μm , includes several distinctive absorption features commonly seen in low mass stars and brown dwarfs: titanium oxide (TiO) and vanadium oxide (VO) as well as calcium hydride (CaH). In general, each of the candidates was given a spectral type based on the depth of the TiO and VO molecular bands (Figures 6, 7, and 8). Note how the TiO absorption features around 7600 and 8400 Å are deeper at later M spectral types (Figures 7 and 8).

To assign spectral types and determine whether a given star is a pre-main sequence member, a background giant, or a foreground dwarf, the spectrum was compared against spectra of standards with known spectral types. These standards included spectra of dwarfs, giants, and the average of a giant and dwarf at a given M spectral type. As demonstrated in Luhman (1999), the depths of the TiO, VO, and CaH molecular bands seen in the pre-main sequence low mass stars are fit well by the average of dwarf and giant spectra. Young stars and brown dwarfs have lower surface gravities than more evolved field dwarfs but do not have surface gravities as low as giants. For objects with spectral types later than M5, averaging a giant and a dwarf result in a good fit because gravity sensitive features seen in field dwarfs are weaker in the spectra of the young stars and brown dwarfs (Luhman 1999). Not all features are dependent on surface gravity. Absorption in VO (at 7900 and 8500 Å), a feature used for spectral classification, is not sensitive to gravity and is therefore similar in dwarfs, giants and young stars with the same spectral type; averaging the dwarf and giant spectra does not significantly change this particular feature. The dwarf and giant standards averaged and used to compare with the OMC 2/3 brown dwarf candidates are referred to throughout this paper as luminosity class IV (and are from Luhman, Liebert, & Rieke 1997; Luhman et al. 1998; Luhman 1999).

As was done by Luhman (1999), the OMC 2/3 spectra were compared with the template dwarf spectra, giant spectra, and the average of a dwarf and a giant spectra. Reddening was also applied to the standards to duplicate the shape of the observed OMC 2/3 sources. The spectral type and luminosity class that provided the best match as judged by visual

inspection was adopted. Since molecular features change rapidly with temperature, the resulting uncertainties in spectral type are ± 0.25 subclass.

Tables 2, 3 and 4 summarize the results of the spectroscopic observations. The tables include: those objects determined to be young brown dwarfs with spectral types later than M6.5 (Table 2), young, low mass members with spectral types of M4–M6 (Table 3) and field dwarfs or giants and sources whose spectral types could not be determined (Table 4).

Of the seven candidates observed with LRIS, three candidates are young M6.5 members (see Figure 6), three were determined to be low mass stars in OMC 2/3, and one is a field dwarf, best matching a M3.25 dwarf spectrum (see Table 4). For the MMT Blue Channel Spectrograph observations, of the twelve candidates observed, three were determined to be young with spectral types ranging from M7–M9; therefore, they are young, brown dwarfs. Eight of the remaining nine are low mass stars with spectral types ranging from M5–M6 and the ninth was determined to be a M2.5 field dwarf. Finally, of the thirteen candidates observed with the MMT Red Channel Spectrograph, three of them are young brown dwarfs with spectral types later than M6.5 (they are also shown in Figure 7), five are young, low mass stars with spectral types ranging from M4–M6, and the remaining five are undetermined. Figure 8 shows the far-red spectra of the remaining M4–M6 members and Figure 9 shows the remaining sources that appear in Table 4.

5.1.2. $H\alpha$ Emission

Strong $H\alpha$ emission is a distinguishing feature of many young pre-main sequence stars, and similarly young substellar objects (e.g. Muzerolle et al. 2005), and its presence in a stellar spectrum is an indication of accretion onto a star from the surrounding disk. In general, the strength of $H\alpha$ emission defines the difference between weak-line T Tauri stars and classical T Tauri stars, i.e. it indicates whether an object is actively accreting material or not. Line strength is measured here by its equivalent width which indicates whether the $H\alpha$ emission is produced from gas accretion or originates from chromospheric activity. Traditionally, a WTTS is defined as having $EW[H\alpha] > -10 \text{ \AA}$ and an $EW[H\alpha] < -10 \text{ \AA}$ is considered to be an actively accreting classical T Tauri star (CTTS). However, here we will use an updated definition of a CTTS, developed by White & Basri (2003) to have $EW[H\alpha] \leq -20 \text{ \AA}$ for those objects with M3–M5.5 spectral types and $EW[H\alpha] \leq -40 \text{ \AA}$ for those with M6–M7.5 spectral types. Although stars with $EW[H\alpha] > -40 \text{ \AA}$ may still be accreting, we cannot distinguish between accretion and chromospheric activity without resolving the $H\alpha$ line and measuring its velocity width.

The best examples of $H\alpha$ emission at 6563\AA can be seen in all three far-red spectra in Figure 6 and in the spectra of candidates 17 and 21 in Figure 7. In particular, candidate 21 exhibits an equivalent width for $H\alpha$ stronger than -100\AA , which with a M7 spectral type indicates that it is an actively accreting young brown dwarf. Based on the White & Basri (2003) definition, however, the three M6.5 brown dwarfs that show $H\alpha$ emission in Figure 6 have $\text{EW}[H\alpha]$ greater than -40\AA and may not be accreting. Table 2 indicates the $H\alpha$ equivalent widths for all the spectroscopically confirmed brown dwarfs.

There are five low mass members with spectral types ranging from M4–M6 which also show detectable $H\alpha$ emission (for values of $\text{EW}[H\alpha]$, see Table 3). Three of the five have $\text{EW}[H\alpha] \leq -20\text{\AA}$, therefore they can be considered to be classical T Tauri stars. The remaining two are likely weak-line T Tauri stars based on their equivalent widths, but to be sure, the Li I (at 6708\AA) absorption abundance should be known (e.g. Martín 1997). Higher resolution spectra would be useful for confirmation of this distinction.

White & Basri (2003) note that low resolution spectra such as the spectra discussed here often overestimate the equivalent width of $H\alpha$ for mid-M and cooler objects. Because the feature is located near the 6569\AA TiO absorption band, at low resolution the $H\alpha$ feature can combine with the edge of the TiO band on one side leading to the underestimation of the continuum, and therefore an overestimation of the equivalent width. In the case of candidate 21, $\text{EW}[H\alpha] < -40\text{\AA}$, and its identification as an actively accreting young brown dwarf appears to be secure.

5.1.3. *Li I, K I, Na I, & Ca II Absorption*

Several atomic absorption features in the optical can be used to establish the youth of the observed candidates: these include Li I, K I, Na I, and Ca II. The detection of lithium provides verification of youth for pre-main sequence stars or verification of substellar mass for field dwarfs. In most of our far-red spectra, lithium is not detected due to the low spectral resolution and modest signal-to-noise of our spectra. The Keck LRIS spectra show Li I in two of the stellar sources (candidates 5 and 6.n in Table 3) confirming the youth of these two pre-main sequence stars. However, for the faint young brown dwarfs observed with Keck (candidates 1, 2 and 3 in Table 2), the signal-to-noise ratio was too low for Li I detection. In addition, Kirkpatrick et al. (2006) caution that the strength of the Li I line is gravity dependent and therefore is not a useful test of the substellar nature of young brown dwarfs.

In the spectra obtained with the Red and Blue Channel Spectrographs at the MMT, K I ($\sim 7700\text{\AA}$) and Na I ($\sim 8200\text{\AA}$) absorption are detected and these lines are good for

discriminating young members of OMC 2/3 from field dwarfs. Both lines are sensitive to gravity, both being much weaker in young, low gravity objects than in higher gravity field dwarfs (as compared in Figure 2 of Luhman et al. 2003). The spectra in Figure 7 show that both absorption features are extremely weak when detected in the probable OMC 2/3 objects identified in Section 5.1.1, further confirming that these are young stars. In order to distinguish from background giants which have even lower surface gravities than young members, the Ca II triplet ($\sim 8500\text{--}8660\text{ \AA}$) can be used as a discriminator: strong Ca II absorption is indicative of giants. However, the Ca II triplet is not detected in any of the spectra.

5.2. Near-Infrared Spectra

5.2.1. *SpeX* Spectra

There have been 56 brown dwarf candidates observed to date with *SpeX*; four of those sources were also observed in the far-red and discussed in the previous section. The 10 members that have spectral types of M7–M9 are summarized in Table 2 and the 4 members with spectral types of M4–M6 are summarized in Table 3. The remaining foreground/background non-members are summarized in Table 4 along with sources of indeterminate type for which spectra have been obtained. Many of the objects listed in Table 4 have relatively featureless spectra (no detectable water absorption features) at this resolution ($\lambda/\Delta\lambda \sim 250$) and are likely reddened field dwarfs or giants. In addition to the brown dwarf candidates, two dozen standards classified from far-red spectra were observed with *SpeX* for comparison with the candidates in order to quantify the shape of the water absorption features indicative of late M-type stars.

Near-infrared spectra of late M (and L) dwarfs are dominated by H₂O absorption bands at 1.4 and 1.85 μm . These steam absorption bands characterize late M dwarfs by broad, plateau-like features in the spectrum (Reid et al. 2001; Leggett et al. 2001). However, young stars and brown dwarfs look quite different in that they exhibit sharp, triangular shaped peaks in the *H*– and *K*–bands (Lucas et al. 2001). The sharp peaks in the *H*–band are possibly due to a reduction in H₂ collision induced absorption (Kirkpatrick et al. 2006). As shown in Figure 10, the shape of the *H*–band peak is strongly dependent on surface gravity, and appears to show distinct shapes for field dwarfs, pre-main sequence stars and giants.

Figure 10 displays a representative sample of the grid of pre-main sequence star and young brown dwarf standards used to classify the candidate brown dwarfs in OMC 2/3. The grid of standards was compiled from Taurus and IC 348 spectra obtained with *SpeX*

as part of this study (see Section 4.2.1) as well as those obtained by Luhman (2006) and Muench et al. (2007). Each candidate spectrum was compared to each spectrum in the grid of standards, reddened using the following interstellar extinction law from Draine (1989):

$$A_\lambda \propto \lambda^{-1.75}. \quad (4)$$

A custom IDL routine computed the value of chi-square for each template reddened by a range of extinction values and selected the one that minimized chi-square as the best fit. The Draine (1989) extinction law was used, and although there is some variation in the value of the exponent of the extinction law in the literature, we find that the derived spectral types do not depend on the precise value of the exponent. In addition, a particular spectral range can be chosen for the fit; however, in general most of the entire spectral range for SpeX was used for classification of these spectra: 0.9–2.4 μm . The result, shown in Figure 11, is a best fit standard spectrum (plus A_V), overplotted on the verified M4–M9 low mass members in OMC 2/3.

Figure 12 illustrates the triangular shaped peaks in the near-infrared spectrum of candidate 29 in OMC 2/3, which was classified as M8–M8.25 from its far-red spectrum. The best fit spectral type from the near-infrared spectrum is M8.5 with an $A_V = 0.5$. Because of these triangular shaped features, it is relatively easy to distinguish between young members and foreground dwarfs or background giants that may contaminate the candidate sample. By varying the spectral type of the standard being used for the fit (as shown in Figure 12), we estimate an uncertainty in spectral class of ± 0.5 subclass.

In addition to candidate 29, several other low mass members, specifically candidates 30, 5 and 75, were observed in the far-red and with SpeX. For candidate 30, the best fit near-infrared type is M7.25 and the far-red type, M7. Candidate 5 has a near-infrared type of M4.75 and a far-red type of M4.75; both spectra indicate that this is a low mass member of OMC 2/3. Candidate 75 has a best fit near-infrared type of M5.75–M6 and the far-red type is M6. In general, near-infrared spectral types of candidates with existing far-red spectra give spectral types within 0.5 subclass of the far-red spectral type. The spectra for candidate 30 is shown (as a spectral template for sources 1004_979 and 845_236) in Figure 11 and candidates 5 and 75 are shown in Figure 13. Spectra for all the sources of indeterminate type (see Table 4) observed with SpeX can be found in both Figures 13 and 14.

5.2.2. *CorMASS Spectra*

Spectral classification for the CorMASS spectra used the same method as for the SpeX spectra, though the regions of the spectra dominated by absorption from telluric water vapor were noisier in the CorMASS spectra and so were removed during the classification process. Figure 15 shows five of the six near-infrared spectra obtained with CorMASS; in two of the cases the spectra obtained were for sources already classified from far-red spectra. Candidate 31, which we found to have a far-red spectral type of M7.75, has a near-infrared spectral type from CorMASS data of M7.5. For the other source, candidate 21, the CorMASS and far-red spectral types are also within 0.25 subclasses.

To demonstrate that the CorMASS spectra can be classified using the SpeX standard spectra, we compared candidates 21 and 30, both of which have far-red spectral types of M7. Candidate 21 was observed with CorMASS and candidate 30 was observed with SpeX. As illustrated in Figure 15, these spectra have virtually identical shapes: candidate 30 looks like candidate 21, reddened with an $A_V=4$. Therefore we maintain that the SpeX spectra and CorMASS spectra are comparable, within 0.25 subclasses. It is useful to note that this was also seen in Luhman et al. (2006) and Allers et al. (2007).

The remaining spectra obtained with CorMASS that did not overlap with previous far-red or SpeX observations are also illustrated in Figure 15. The source d216-0939 was imaged by Smith et al. (2005) with Advanced Camera for Surveys on the Hubble Space Telescope as a nearly edge-on disk. Its near-infrared spectrum, shown in Figure 15, is shown with a young M3 star over-plotted. It is clear that the spectral type of this source is earlier than M3. However, since we do not have template near-infrared spectra for young stars with spectral types earlier than M3, we were unable to precisely determine the type. In addition, when we compared d216-0939 with field dwarfs earlier than M3, it was difficult to match the shape of these sources with the shape of d216-0939 because of a near-infrared excess which we attribute to the disk. Therefore, this object is classified as having an indeterminate type and is listed in Table 4.

The CorMASS spectrum of CHS 9695 indicates that it is a highly reddened object (see Figure 15). Although the spectrum very closely matches a spectrum of a young M3 object, it is slightly shallower and therefore, as with d216-0939, we were also unable to precisely determine its type (see Table 4). The candidate CHS 8782 was successfully classified from its CorMASS spectrum through our comparison method as a member of OMC 2/3 with a spectral type of M5.25. One additional candidate, 583.352 has a CorMASS spectrum with very low signal-to-noise and therefore we are unable to confidently determine a spectral type.

6. Discussion

Spectra have been obtained for 88 candidate low mass members in OMC 2/3, of which 40 new low mass members with spectral types of M4–M9 have been identified. Of those, 19 have spectral types later than M6.5, making them *bona fide* young brown dwarfs. As seen in Figure 1, the spatial distribution of the young brown dwarfs as compared with the low mass M4–M6 sources is fairly similar.

We have observed all the brown dwarf candidates that fall below $0.080 M_{\odot}$ and above $0.050 M_{\odot}$ (for 1 Myr objects), and with an extinction limit of $4.5 < A_V < 14$, making a complete sample within this regime (see Figure 4). Within these parameters lie a total of 22 candidates and of those, 11 are spectroscopically confirmed members with spectral types of M4–M9, and 11 are objects of indeterminate type (one of which, 583_352, might be a member but a higher signal-to-noise spectrum is necessary for confirmation). Therefore we find that $\sim 50\%$ of candidates detected within this range of extinction and dereddened magnitude are members.

6.1. The H-R Diagram

In order to determine the masses and ages of our sample, we estimate the effective temperatures and bolometric luminosities for the 40 low mass members and place them on an H-R diagram. The effective temperature, T_{eff} , for each source was determined from its spectral type using the temperature scale of Luhman et al. (2003). We used the $J - H$ color to determine the reddening and dereddened the H -band magnitude; then the bolometric correction was applied. The methodology is described in detail in Appendix A.

It is important to note that the A_V values used to compute the dereddened H -band magnitude are not based on the ones found from spectral classification, but are based on the $J - H$ color. The reason for this is that the standard spectra used for comparison are the *observed spectra* and have not been dereddened. Although the A_V values for these sources are low (likely $A_V < 2$), we wanted to deredden all the spectra uniformly and therefore chose to do so using the $J - H$ color.

Figure 16 shows the resulting effective temperatures and bolometric luminosities for the OMC 2/3 members on an H-R diagram (note that only 39 of the 40 low mass members appear on the diagram because source 774_120 does not have a J -band magnitude and so its bolometric luminosity could not be calculated in the same way as the others). Overplotted are the 1, 3, and 10 Myr isochrones from Baraffe et al. (1998). These isochrones are appropriate since we have adopted the temperature scale of Luhman et al. (2003) which

has been calibrated for use with these isochrones. Based on these evolutionary tracks, we estimate the 40 members with M4–M9 spectral types to range in mass from 0.35–0.015 M_{\odot} . In general, though, the evolutionary models at present do not extrapolate consistent masses for sources with masses below the hydrogen burning limit (Hillenbrand & White 2004). An additional uncertainty in the H-R diagram of OMC 2/3 lies in the adopted distance of 450 pc. Using the more recent value of 420 pc (e.g. Menten et al. 2007) instead of 450 pc shifts the points down on the H-R diagram, to later ages, by a value of $\log(L_{bol}/L_{\odot}) \sim 0.06$.

Seventeen of the nineteen sources with spectral types later than M6.5 are located above the 1 Myr track. However, two of them (candidates 21 and 845_236) sit well below the 3 Myr track. For the 21 members with spectral types between M4 and M6, 11 of them fall either very close to the 1 Myr isochrone or between the 1 and 3 Myr isochrones, and there are 8 likely members that fall very close to, or below the 3 Myr isochrone. Although there are several sources that appear clustered at an age below the 3 Myr isochrone on the H-R diagram, this is primarily due to a selection effect from our requirement that the luminosity of our candidates be less than that of a 1 Myr brown dwarf. Without spectral types for the more luminous sources in OMC 2/3, we cannot determine whether these ages are typical, or whether most of the stars are indeed above 1 Myr in age. We have detected one M4 source above the 1 Myr isochrone; this source serendipitously fell into the slit during our observations and was not in the sample selected from our photometry.

Also shown in Figure 16 are the CorMASS sources CHS 9695, a source which is variable (and hence a likely member), as seen by Carpenter, Hillenbrand, & Skrutskie (2001), and d216-0939, the edge-on disk discovered by Smith et al. (2005). Since we have assigned an upper limit of M3 for the spectral types for these two objects (see Table 4), the locations of these sources on the H-R diagram are plotted for spectral classifications of M1, M2 and M3. CHS 9695 is clearly young, falling well above the 1 Myr track for all three spectral types. The edge-on disk, d216-0939, falls between the 3 Myr and 10 Myr tracks for all three spectral types. We caution that the possibility of strong veiling for d216-0939 in the 1–1.8 μm regime could result in a significant overestimation in the temperature of this object.

The fact that d216-0939, as well as candidates 21 and 845_236 mentioned above, appear older than 3 Myr on the H-R diagram suggests that it is possible these sources are underluminous and young but appear older on the H-R diagram due to an obscuring disk. Disks may absorb the light of the star, particularly if they are highly flared (Walker et al. 2004); however, the star may not appear unusually red due to a strong contribution of light scattered off the disk. Hubble Space Telescope images of d216-0939 show a strong contribution from scattered light in this system (Smith et al. 2005). In support of this, candidate 21 shows strong $H\alpha$ emission, suggesting that it has an accretion disk.

To obtain a more accurate estimate of the age of OMC 2/3, we need spectra of candidate members with types earlier than M6 and with luminosities above our luminosity limit to fill in that portion of the H-R diagram. With the H-R diagram we currently have, we can make the following observations. First, eighteen of the forty OMC 2/3 sources (45%), and in particular, seventeen of the nineteen (89%) young brown dwarfs, are located above the 1 Myr isochrone. Therefore we estimate an age for OMC 2/3 of approximately 1 Myr. Second, although many of the members are close to or above the 1 Myr isochrone, we clearly detect a range of ages along the line-of-sight to OMC 2/3. We now examine the implications of this observed age spread.

6.2. Age Spread

The wide range of inferred ages detected in OMC 2/3 is surprising given the high density of protostars, and hence the presumed youth, of this region. There has already been considerable debate on the nature of age spreads in the Orion molecular cloud. Huff & Stahler (2006) find evidence for an age spread of 8–10 Myr in the H-R diagram of stars in the ONC, which they argue is real. Palla & Stahler (1999) find evidence of an increasing (i.e. accelerating) rate of star formation in the ONC which continued to rise until the present time. In their age histogram for stars in the ONC (with masses ranging from 0.4–0.6 M_{\odot}), all stars are less than 10 Myr in age, with most having ages less than 7 Myr. Hartmann (2001), and more recently Hillenbrand, Bauermeister, & White (2007), argue that such age spreads may result from uncertainties in the luminosity, membership, and the pre-main sequence star tracks. In addition, Lodieu et al. (2008) discuss how the presence of multiple systems can result in an age spread in their study of the Upper Sco association. Multiplicity would result in an *underestimate* of the ages. This likely effects only a very small percentage of sources in OMC 2/3 since the companion star fraction in the outskirts of the ONC for low mass PMS sources ($\lesssim 5\%$; Köhler et al. 2006) has been found to be much lower than in other star-forming regions (a factor of 5 lower than in Upper Sco).

In a study of low mass stars and brown dwarfs in the ONC, Slesnick, Hillenbrand, & Carpenter (2004) see two populations toward the ONC: a young, $\lesssim 1$ Myr population and an older, 10 Myr population. However, in a more recent study of 45 new members of the Trapezium, an older, 10 Myr population of stars was not seen (Riddick, Roche, & Lucas 2007); they suggest this may be the result of their source selection. Although we do not see a clear bifurcation into two populations as in Slesnick, Hillenbrand, & Carpenter (2004), our H-R diagram for the neighboring OMC 2/3 region shows a significant age spread as well. Understanding the age spread in OMC 2/3 can bring new insight into the debate over the age

spreads observed in Orion as a whole.

It is important to note that we rule out that the age spread seen is due to an error in spectral classification. All candidates determined to be members in OMC 2/3 show low surface gravity features in their spectra that rule out the possibility that they are foreground M dwarfs. In addition, the photometric uncertainty is small and any variability is likely on the order of tenths of magnitudes, not several magnitudes as would be required to change the H-R diagram significantly. One possible source of uncertainty lies in our method of using a constant intrinsic $J - H$ color to calculate the color excess for each source (see Appendix A); however, to test this, we plotted the same H-R diagram using the intrinsic $J - H$ values for each spectral type presented in Leggett (1992, using the young disk population types found in their Table 6). Using the values presented in that table instead of a constant intrinsic $J - H$ color for all spectral types shifts the location of the sources with spectral types of M7.5 and later slightly closer to the 1 Myr isochrone, but does not shift them to ages older than 1 Myr.

We consider here several reasons for the spread of ages seen in OMC 2/3: confusion with members of the older subgroups in the Orion OB 1 association, uncertainties in the determination of luminosity and spectral type due to extinction from a disk, veiling, and finally, the presence of a *bona fide* age spread.

First, we assess the possibility of contamination from older members of the OB 1 association by examining the number of sources in each age range versus the amount of extinction toward that object (see Figure 17). All 40 low mass members with spectral types ranging from M4–M9 are included, as well as the two CorMASS sources with upper limits to their spectral types of M3. The sources are grouped into three categories: those with ages on the H-R diagram < 1 Myr, those with ages 1–3 Myr, and those with ages > 3 Myr. The low extinction values for the 1–3 Myr sources may indicate we are seeing a foreground population; or perhaps we are seeing the older, Orion OB 1c association which is 4.6 Myr old (Brown, de Geus, & de Zeeuw 1994) and falls along the line-of-sight of OMC 2/3. However, it seems unlikely that the sources greater than 3 Myr are foreground since they are, for the most part, more embedded. We cannot completely rule out this scenario because some of the older stars may show extinction due to circumstellar dust or from dust located within the Orion OB association but outside the molecular cloud. Furthermore, some older stars could be trapped within the Orion molecular cloud, as suggested by Pflamm-Altenburg & Kroupa (2007).

Second, as discussed before, a combination of extinction and scattering from a nearly edge-on, flared circumstellar disk could result in the luminosity of a star being underestimated. Since this would depend on the presence of a disk, as well as its inclination, the effect

of disks could result in both increased scatter and an overestimated age. The > 3 Myr sources d216-0939, candidate 21, and candidate 845_236 are possible examples of sources which appear underluminous due to the presence of a disk; these examples make this perhaps the most likely of these scenarios. As additional support for this scenario, at least three of the ~ 10 Myr sources in the ONC are known proplyds or silhouette disks, and therefore younger than their positions on the H-R diagram suggest (Slesnick, Hillenbrand, & Carpenter 2004; Riddick, Roche, & Lucas 2007).

Third, excess emission from nonphotospheric sources in the J - and H -bands may effect our estimates of both luminosity and effective temperature. Cieza et al. (2005) find that for classical T Tauri stars, J - and H -band luminosities are consistently overestimated, leading to an underestimation in age. If we are to assume that there is significant J - and H -band excess in our OMC 2/3 sources which we have not accounted for, then this would imply that we have overestimated the photospheric luminosity of the sources and that the ages are systematically underestimated. This could increase the observed age spread by shifting sources with higher accretion rates to younger inferred ages; however, this would also imply that many sources are older than they appear on the H-R diagram. In this case the mass, particularly of the brown dwarfs, would stay relatively constant since the mass tracks are virtually vertical at these ages (see Figure 16). Near-infrared excess could also cause veiling and potentially bias sources to earlier types by reducing the observed depth of the water features. Although we find some evidence for K -band excesses in the color-color diagram, we find no evidence for excesses in the spectra given the excellent fits in the near-infrared spectra and the consistency between the far-red and near-infrared spectral types. Therefore, there is no clear evidence for veiling and significant excess emission in the J - and H -bands.

Finally, it is possible that the age spread we see in OMC 2/3 is real. This is the conclusion drawn by Palla et al. (2005) based on their study of lithium depletion in the ONC. They find low mass members of the ONC with ages $\gtrsim 10$ Myr, which is much older than many of the stars in this region, and indicate that this may mean the star formation history of the cluster has a much longer duration than previously thought. Jeffries (2007b) used rotation periods and equatorial velocities of known PMS stars in the ONC to model the distribution of their projected radii and in turn, the distribution of ages. The simulations showed that an age spread of 1–3 Myr in the low-luminosity ONC members is consistent with the data, independent of the evolutionary models used. However, the older stars discovered in the conventional H-R diagram analysis were not present in his analysis. Jeffries concluded that he could not verify the presence of the 10 Myr sources.

In order to determine which of these possibilities is most likely in OMC 2/3, future studies should examine the ages of the stars above the hydrogen burning limit to see if

most stars in OMC 2/3 have ages around 1 Myr, similar to the brown dwarfs, or if an age spread is seen in the higher mass PMS stars as well. With such a complete sample, we could potentially fully understand the star formation history of OMC 2/3.

7. Conclusions

Forty new low mass members with spectral types of M4–M9 have been spectroscopically confirmed in OMC 2/3. Using deep, I –, z' –, J –, H – and K –band photometry of a $20' \times 20'$ field in OMC 2/3, we selected candidates with luminosities and colors consistent with brown dwarfs for follow-up spectroscopy. Low resolution, far-red and near-infrared spectra were obtained for a sample of candidates and 19 objects with spectral types of M6.5–M9 and 21 objects with spectral types of M4–M6 were confirmed by fitting these spectra to standard spectra, and presented. These spectral types correspond to masses of 0.35–0.015 M_{\odot} using the evolutionary models of Baraffe et al. (1998) and we estimate an age for OMC 2/3 from the substellar members of approximately 1 Myr. However, a significant fraction of selected low luminosity sources are pre-main sequence stars with ages ranging from 1–10 Myr.

We discussed several reasons for the age spread we see in OMC 2/3. First, that the older stars are part of the OB 1c association in the foreground to the Orion A cloud. Although this possibility has not been ruled out, we find it unlikely because the older stars seem to be embedded in the Orion molecular cloud, as was found for the older stars in the ONC (Slesnick, Hillenbrand, & Carpenter 2004). Second, that the measurement of the ages are effected by uncertainties in the luminosity of the sources. Our data exhibit some evidence that the presence of disks can lead to overestimating the age of the sources. For example, the apparent old ages of the edge-on disk d216-0939 and the strongly accreting candidate 21 may be explained by the presence of an edge-on or nearly edge-on flared disk which is obscuring the star. Finally, it is possible that we are observing a *bona fide* age spread in OMC 2/3.

We are grateful to N. Caldwell for the Blue Channel Spectrograph observations and J. Rayner and B. Bus for help with SpeX observations. We also thank M. Cushing for help with Spextool/Cormasstool and M. Merrill for providing some SQIID calibration data and help understanding SQIID linearity. Finally, thanks go to the anonymous referee whose useful comments have improved this paper. Support for STM was provided in part by NASA through contract 1256790 issued by JPL/Caltech. CorMASS is supported by a generous gift from the F.H. Levinson Fund of the Peninsula Community Foundation. The authors also wish to recognize and acknowledge the very significant cultural role and reverence that the

summit of Mauna Kea has always had within the indigenous Hawaiian community. We are most fortunate to have the opportunity to conduct observations from this mountain. This research has made use of NASA’s Astrophysics Data System.

Facilities: ARC (CorMASS), FLWO:1.2m (4-Shooter), IRTF (SpeX), Keck:I (LRIS), KPNO:2.1m (SQIID), MMT (Red & Blue Channel Spectrographs), VATT (CorMASS), Magellan:Clay (CorMASS)

A. Bolometric Luminosity and Effective Temperature

Spectral types of stars and brown dwarfs correspond to an estimate of the atmospheric effective temperature (T_{eff}). The specific effective temperatures are associated with spectral types (which we identify) and such a correspondence has been provided in the literature (Luhman et al. 2003). Photometric observations are used to ascertain the bolometric luminosity of each star and brown dwarf candidate. T_{eff} and L_{bol} are then compared against theoretical evolutionary models for a range of masses.

In order to assess the bolometric luminosity for each source, we take the following steps:

- Compute the excess in the $J - H$ color, $E(J - H)$, for each of the stars and brown dwarfs.

$$E(J - H) = (J - H) - (J - H)_0 \tag{A1}$$

where $(J - H)_0 = 0.6$. This value is representative of the intrinsic $J - H$ colors given for young, M stars (ranging from M0–M9) in Table 6 of Leggett (1992).

- The extinction, A_H can be obtained from the color excess:

$$\frac{E(J - H)}{A_V} = \frac{A_J}{A_V} - \frac{A_H}{A_V} = 0.11 \tag{A2}$$

where values for A_λ/A_V are from Cohen et al. (1981). Specific A_H values for each of the candidates are listed in column 10 in Tables 2, 3 and 4. Note that these values of A_H are calculated from photometric observations, and not calculated from the A_V values found as the best fit for spectral classification.

- Compute the apparent bolometric magnitude m_{bol} for each star and brown dwarf. This can be done at any wavelength; here we use H -band. The bolometric corrections are taken from a variety of sources in the literature for M dwarfs, corrected

appropriately for filter transformations. For the M1-M4 and M6 spectral types, values from Kenyon & Hartmann (1995, see Table A5) were used. For M5, an average of values from Kenyon & Hartmann (1995), Bessell (1991), and Leggett et al. (1996) were used. For M7, an interpolation of values given in Kenyon & Hartmann (1995) and Leggett et al. (1996) was used. And finally, for M8-M9, values from Tinney, Mould, & Reid (1993) were used.

$$m_{bol} = BC_H + H - A_H \quad (\text{A3})$$

- Finally, $\log(L_{bol}/L_{\odot})$, the values that are plotted in Figure 16, can be computed:

$$\log\left(\frac{L_{bol}}{L_{\odot}}\right) = \frac{4.76 - m_{bol} + 5 \log d - 5}{2.5} \quad (\text{A4})$$

where $d = 450$ pc.

REFERENCES

- Allers, K. N., Jaffe, D. T., Luhman, K. L., Liu, M. C., Wilson, J. C., Skrutskie, M. F., Nelson, M., Peterson, D. E., Smith, J. D., & Cushing, M. C. 2007, *ApJ*, 657, 511
- Bally, J., Langer, W. D., Stark, A. A., & Wilson, R. W. 1987, *ApJ*, 312, L45
- Baraffe, I., Chabrier, G., Allard, F., & Hauschildt, P. H. 1998, *A&A*, 337, 403
- Bessell, M. S. 1991, *AJ*, 101, 662
- Bessell, M. S. & Brett, J. M. 1988, *PASP*, 100, 1134
- Briceño, C., Luhman, K. L., Hartmann, L., Stauffer, J. R., & Kirkpatrick, J. D. 2002, *ApJ*, 580, 317
- Brown, A. G. A., de Geus, E. J., & de Zeeuw, P. T. 1994, *A&A*, 289, 101
- Carpenter, J. M., Hillenbrand, L. A., & Skrutskie, M. F. 2001, *AJ*, 121, 3160
- Chabrier, G. & Baraffe, I. 1997, *A&A*, 327, 1039
- Chini, R., Reipurth, B., Ward-Thompson, D., Bally, J., Nyman, L.-A., Sievers, A., & Billawalla, Y. 1997, *ApJ*, 474, L135

- Cieza, L. A., Kessler-Silacci, J. E., Jaffe, D. T., Harvey, P. M., & Evans, N. J. 2005, *ApJ*, 635, 422
- Cohen, J. G., Frogel, J. A., Persson, S. E., & Elias, J. H. 1981, *ApJ*, 249, 481
- Cushing, M. C., Vacca, W. D., & Rayner, J. T. 2004, *PASP*, 116, 362
- Draine, B. T. in *Proc 22nd Eslab Symposium on Infrared Spectroscopy in Astronomy*, ESA SP-290, 1989, 93
- Ellis, T., Drake, R., Fowler, A. M., Gatley, I., Heim, J., Luce, R., Merrill, K. M., Probst, R., & Buchholz, N. 1992, *Proc. SPIE*, 1765, 94
- Genzel, R. & Stutzki, J. 1989, *ARA&A*, 27, 41
- Gutermuth, R. A., Megeath, S. T., Muzerolle, J., Allen, L. E., Pipher, J. L., Myers, P. C., & Fazio, G. G. 2004, *ApJS*, 154, 374
- Hartmann, L. 2001, *AJ*, 121, 1030
- Hillenbrand, L. A. 1997, *AJ*, 113, 1733
- Hillenbrand, L. A., Bauermeister, A., & White, R. J. 2007, in “Cool Stars 14”, *ASP Conference Series* (arXiv:astro-ph/0703642v1)
- Hillenbrand, L. A. & White, R. J., 2004, *ApJ*, 604, 741
- Hirota, T., et al. 2007, *PASJ*, 59, 897
- Huff, E. M., & Stahler, S. W. 2006, *ApJ*, 644, 355
- Jeffries, R. D. 2007a, *MNRAS*, 376, 1109
- Jeffries, R. D. 2007b, *MNRAS*, 381, 1169
- Johnson, J. J., Gehrz, R. D., Jones, T. J., Hackwell, J. A., & Grasdalen, G. L. 1990, *AJ*, 100, 518
- Kenyon, S. J., & Hartmann, L. 1995, *ApJS*, 101, 117
- Kirkpatrick, J. D., Reid, I. N., Liebert, J., Gizis, J. E., Burgasser, A. J., Monet, D. G., Dahn, C. C., Nelson, B., & Williams, R. J. 2000, *AJ*, 120, 447
- Kirkpatrick, J. D., Barman, T. S., Burgasser, A. J., McGovern, M. R., McLean, I. S., Tinney, C. G., & Lowrance, P. J. 2006, *ApJ*, 639, 1120

- Köhler, R., Petr-Gotzens, M. G., McCaughrean, M. J., Bouvier, J., Duchêne, G., Quirrenbach, A., & Zinnecker, H. 2006, *A&A*, 458, 461
- Landolt, A. U. 1992, *AJ*, 104, 340
- Leggett, S. K. 1992, *ApJS*, 82, 351
- Leggett, S. K., Allard, F., Berriman, G., Dahn, C. C., & Hauschildt, P. H. 1996, *ApJS*, 104, 117
- Leggett, S. K., Allard, F., Geballe, T. R., Hauschildt, P. H., & Schweitzer, A. 2001, *ApJ*, 548, 908
- Lis, D. C., Serabyn, E., Keene, J., Dowell, C. D., Benford, D. J., Phillips, T. G., Hunter, T. R., & Wang, N. 1998, *ApJ*, 509, 299
- Lodieu, N., Hambly, N. C., Jameson, R. F., & Hodgkin, S. T. 2008, *MNRAS*, 383, 1385
- Lucas, P. W., Roche, P. F., Allard, F., & Hauschildt, P. H. 2001, *MNRAS*, 326, 695
- Luhman, K. L. 1999, *ApJ*, 525, 466
- Luhman, K. L. 2000, *ApJ*, 544, 1044
- Luhman, K. L., Briceño, C., Rieke, G. H., & Hartmann, L. 1998, *ApJ*, 493, 909
- Luhman, K. L., Liebert, J., & Rieke, G. H. 1997, *ApJ*, 489, L165
- Luhman, K. L., Stauffer, J. R., Muench, A. A., Rieke, G. H., Lada, E. A., Bouvier, J., & Lada, C. J. 2003, *ApJ*, 593, 1093
- Luhman, K. L. 2006, *ApJ*, 645, 676
- Luhman, K. L., Wilson, J. C., Brandner, W., Skrutskie, M. F., Nelson, M. J., Smith, J. D., Peterson, D. E., Cushing, M. C., & Young, E. 2006, *ApJ*, 649, 894
- Martín, E. L. 1997, *A&A*, 321, 492
- Menten, K. M., Reid, M. J., Forbrich, J., & Brunthaler, A. 2007, *A&A*, 474, 515
- Meyer, M. R., Calvet, N., & Hillenbrand, L. A. 1997, *AJ*, 114, 288
- Muench, A. A., Lada, C. J., Luhman, K. L., Muzerolle, J., & Young, E. 2007, *AJ*, 134, 411
- Muzerolle, J., Luhman, K. L., Briceño, C., Hartmann, L., & Calvet, N. 2005, *ApJ*, 625, 906

- Oke, J.B., Cohen, J.G., Carr, M., Cromer, J., Dingizian, A., Harris, F.H., Labrecque, S., Lucinio, R., Schall, W., Epps H., & Miller, J. 1995, *PASP*, 107, 375
- Palla, F., Randich, S., Flaccomio, E., & Pallavicini, R. 2005, *ApJ*, 626, L49
- Palla, F. & Stahler, S. 1999, *ApJ*, 525, 772
- Pflamm-Altenburg, J. & Kroupa, P. 2007, *MNRAS*, 375, 855
- Rayner, J. T., Toomey, D. W., Onaka, P. M., Denault, A. J., Stahlberger, W. E., Vacca, W. D., Cushing, M. C., & Wang, S. 2003, *PASP*, 115, 362
- Reid, I. N., Burgasser, A. J., Cruz, K. L., Kirkpatrick, J. D., & Gizis, J. E. 2001, *AJ*, 121, 1710
- Reipurth, B., & Clarke, C. 2001, *AJ*, 122, 432
- Riddick, F. C., Roche, P. F., & Lucas, P. W. 2007, *MNRAS*, 381, 1077
- Sandstrom, K. M., Peek, J. E. G., Bower, G. C., Bolatto, A. D., & Plambeck, R. L. 2007, *ApJ*, 667, 1161
- Skrutskie, M. F., Cutri, R. M., Stiening, R., Weinberg, M. D., Schneider, S., Carpenter, J. M., Beichman, C. Capps, R., Chester, T., Elias, J., Huchra, J., Liebert, J., Lonsdale, C., Monet, D. G., Price, S., Seitzer, P., Jarrett, T., Kirkpatrick, J. D., Gizis, J. E., Howard, E., Evans, T., Fowler, J., Fullmer, L., Hurt, R., Light, R., Kopan, E. L., Marsh, K. A., McCallon, H. L., Tam, R., Van Dyk, S., & Wheelock, S. 2006, *AJ*, 131, 1163
- Slesnick, C. L., Hillenbrand, L. A., & Carpenter, J. M. 2004, *ApJ*, 610, 1045
- Smith, N., Bally, J., Licht, D., & Walawender, J. 2005, *AJ*, 129, 382
- Tinney, C. G., Mould, J. R., & Reid, I. N. 1993, *AJ*, 105, 1045
- Vacca, W. D., Cushing, M. C., & Rayner, J. T. 2003, *PASP*, 115, 389
- Walker, C., Wood, K., Lada, C. J., Robitaille, T., Bjorkman, J. E., & Whitney, B. 2004, *MNRAS*, 351, 607
- White, R. J. & Basri, G. 2003, *ApJ*, 582, 1109
- Wiling, B. A., Greene, T. P., & Meyer, M. R. 1999, *AJ*, 117, 469

Wilson, J. C., Skrutskie, M. F., Colonna, M. R., Enos, A. T., Smith, J. D., Henderson, C. P., Gizis, J. E., Monet, D. G., & Houck, J. R. 2001, *PASP*, 113, 227

Yu, K. C., Bally, J., & Devine, D. 1997, *ApJ*, 485, L45

Table 1. Summary of $Iz'JHK$ Photometric Completeness

Filter	Number of Sources ^a	90% Completeness Limits
...	...	[mag]
<i>I</i>	985	18.0 ^b
<i>z'</i>	1092	18.1 ^b
<i>J</i>	1057	18.0
<i>H</i>	1232	17.1
<i>K</i>	1296	16.3

^aNumber of sources in the observed field with photometric uncertainties less than 0.15 magnitudes.

^bThe 90% completeness limit quoted here is for the region north of a declination of -5.15 ; if we include the entire image in our analysis, the magnitude quoted is 80% complete.

Table 2. Summary of Spectral Observations: Brown Dwarfs

Name ...	R. A. ^a (J2000)	Dec. ^a (J2000)	I, σ_I^b (mag)	$z', \sigma_{z'}^b$ (mag)	J, σ_J^c (mag)	H, σ_H^c (mag)	K, σ_K^c (mag)	Sp. Type ...	A_H^i ...	EW[H α] (Å)
1	05 35 27.4	-05 09 04	17.882 ± 0.036	17.398 ± 0.042	14.852 ± 0.009	14.107 ± 0.008	13.594 ± 0.011	M6.5 ^d	0.2	-19.2
2	05 35 16.8	-05 07 27	17.819 ± 0.018	16.903 ± 0.016	14.953 ± 0.009	14.413 ± 0.009	13.947 ± 0.011	M6.5 ^d	0.0	-16.9
3	05 35 13.0	-05 02 09	17.393 ± 0.005	16.257 ± 0.008	14.465 ± 0.007	13.895 ± 0.007	13.477 ± 0.007	M6.5 ^d	0.0	-25.8
29	05 35 12.9	-05 15 49	18.447 ± 0.051	17.441 ± 0.039	15.082 ± 0.015	14.309 ± 0.013	13.806 ± 0.015	M8-M8.25 ^e , M8.5 ^g	0.2	neb ^j
30	05 35 12.7	-05 15 43	18.394 ± 0.069	17.378 ± 0.056	14.825 ± 0.010	13.951 ± 0.010	13.328 ± 0.008	M7 ^e , M7.25 ^g	0.4	neb ^j
31	05 35 18.7	-05 15 18	18.003 ± 0.062	16.369 ± 0.030	14.488 ± 0.009	13.658 ± 0.007	13.077 ± 0.009	M7.75 ^e , M7.5 ^h	0.3	neb ^j
21	05 35 38.2	-05 03 34	18.561 ± 0.018	17.609 ± 0.017	16.112 ± 0.027	15.373 ± 0.031	14.840 ± 0.024	M7 ^f , M7.25 ^h	0.2	-105.1
34	05 35 13.6	-05 14 22	18.445 ± 0.077	17.344 ± 0.051	15.793 ± 0.020	14.880 ± 0.017	14.335 ± 0.022	M8 ^f	0.4	...
77	05 35 40.3	-05 12 32	19.290 ± 0.40?	17.355 ± 0.098	15.462 ± 0.026	14.687 ± 0.018	14.155 ± 0.019	M7 ^f	0.2	...
923_1621	05 35 15.1	-04 58 09	17.867 ± 0.051	16.197 ± 0.028	15.200 ± 0.029	M8 ^g	1.5	...
1036_108	05 35 10.1	-05 14 56	16.551 ± 0.032	15.397 ± 0.022	14.594 ± 0.020	M9 ^g	0.8	...
543_681	05 35 32.0	-05 08 35	16.848 ± 0.026	15.430 ± 0.017	14.485 ± 0.014	M7.25 ^g	1.2	...
766_341	05 35 22.1	-05 12 21	17.035 ± 0.081	15.908 ± 0.040	14.873 ± 0.027	M7.75 ^g	0.7	...
441_326	05 35 36.6	-05 12 31	16.547 ± 0.070	15.758 ± 0.058	14.906 ± 0.051	M8.5 ^g	0.3	...
988_148	05 35 12.2	-05 14 29	17.851 ± 0.069	16.503 ± 0.037	15.304 ± 0.030	M8 ^g	1.1	...
1004_979	05 35 11.5	-05 05 16	16.321 ± 0.019	14.986 ± 0.011	14.330 ± 0.011	M7 ^g	1.0	...
727_1506	05 35 23.9	-04 59 25	18.398 ± 0.070	16.800 ± 0.034	15.842 ± 0.031	M7.75 ^g	1.4	...
845_236	05 35 23.3	-05 13 48	16.714 ± 0.060	15.789 ± 0.037	14.607 ± 0.029	M7 ^g	0.5	...
735_36	05 35 28.2	-05 16 01	15.790 ± 0.049	14.673 ± 0.020	13.978 ± 0.021	M8-M8.25 ^g	0.7	...

^aCoordinates from 2MASS final release.

^bMagnitudes and relative uncertainties from 4-Shooter photometry.

^cMagnitudes and relative uncertainties from SQUID photometry.

^dKeck LRIS spectra.

^eBlue Channel MMT spectra.

^fRed Channel MMT spectra.

^gSpeX IRTF spectra.

^hCorMASS spectra.

ⁱ A_H values calculated from $J - H$ colors (see Appendix A) and not from the A_V values found as the best fit from spectral classification.

^jToo much emission from surrounding HII region to measure H α .

Table 3. Summary of Spectral Observations: Low Mass Members

Name ...	R. A. ^a (J2000)	Dec. ^a (J2000)	I, σ_I^b (mag)	z' , $\sigma_{z'}^b$ (mag)	J, σ_J^c (mag)	H, σ_H^c (mag)	K, σ_K^c (mag)	Sp. Type ...	A_H^i ...	EW[H α] (Å)
4	05 35 25.0	-05 09 10	17.198 ± 0.039	16.374 ± 0.027	14.494 ± 0.007	13.904 ± 0.007	13.505 ± 0.014	M6 ^d	0.0	-17.5
5	05 35 24.1	-05 09 07	16.444 ± 0.022	15.972 ± 0.025	14.374 ± 0.009	13.804 ± 0.007	13.385 ± 0.008	M4.75 ^{d,g}	0.0	-32.6
6.n	05 35 16.2	-05 09 19	14.853 ± 0.002	14.262 ± 0.003	12.916 ± 0.003	12.241 ± 0.003	11.996 ± 0.003	M4.5-M4.75 ^d	0.1	-23.7
13	05 35 12.7	-05 12 01	16.471 ± 0.008	15.655 ± 0.005	14.164 ± 0.006	13.535 ± 0.006	13.243 ± 0.007	M5.5 ^e	0.0	...
15	05 35 35.7	-05 10 51	16.360 ± 0.004	15.633 ± 0.005	14.380 ± 0.007	13.768 ± 0.006	13.381 ± 0.008	M5.5 ^e	0.0	...
17	05 35 42.7	-05 10 16	17.234 ± 0.030	16.393 ± 0.030	14.833 ± 0.010	14.233 ± 0.010	13.784 ± 0.011	M5.5 ^f	0.0	-36.4
18	05 35 15.6	-05 09 32	16.114 ± 0.004	15.411 ± 0.005	13.943 ± 0.006	13.340 ± 0.005	13.023 ± 0.006	M5.75 ^e	0.0	...
20	05 35 37.0	-05 05 26	17.164 ± 0.024	16.247 ± 0.015	14.702 ± 0.008	14.128 ± 0.007	13.701 ± 0.008	M6-M6.25 ^e	0.0	...
23	05 35 40.0	-05 02 37	16.239 ± 0.002	15.482 ± 0.003	14.111 ± 0.006	13.489 ± 0.006	13.159 ± 0.006	M5.5 ^e	0.0	-16.4
24	05 35 19.7	-05 02 29	16.927 ± 0.007	16.088 ± 0.011	14.502 ± 0.007	13.882 ± 0.007	13.524 ± 0.007	M5.75 ^e	0.0	...
27	05 34 43.5	-05 14 43	16.889 ± 0.015	16.189 ± 0.011	14.894 ± 0.009	14.115 ± 0.008	13.697 ± 0.008	M5 ^e	0.3	...
33	05 35 16.8	-05 14 47	18.041 ± 0.079	16.855 ± 0.040	15.257 ± 0.013	14.255 ± 0.010	13.636 ± 0.012	M5.5 ^f	0.6	...
70	05 35 16.3	-05 04 36	16.805 ± 0.005	16.061 ± 0.012	14.621 ± 0.008	13.974 ± 0.007	13.729 ± 0.008	M5.5 ^e	0.1	...
75	05 34 44.9	-05 12 32	18.732 ± 0.039	17.419 ± 0.033	15.324 ± 0.014	14.327 ± 0.012	13.752 ± 0.014	M6 ^f , M5.75 ^g	0.6	...
76	05 35 20.2	-05 12 11	16.623 ± 0.073	15.660 ± 0.036	14.978 ± 0.010	14.102 ± 0.009	13.630 ± 0.009	M5.5 ^f	0.4	...
78	05 34 56.7	-05 13 57	19.444 ± 0.209	18.170 ± 0.112	15.901 ± 0.015	14.805 ± 0.011	14.297 ± 0.011	M4.5 ^f	0.7	...
636_972	05 35 32.6	-05 05 38	18.011 ± 0.032	17.174 ± 0.034	15.805 ± 0.014	14.791 ± 0.010	14.164 ± 0.011	M4.25 ^g	0.6	...
369_674	05 35 44.5	-05 08 56	...	19.125 ± 0.251	16.149 ± 0.021	14.831 ± 0.012	14.073 ± 0.011	M4.25 ^g	1.0	...
774_120	05 35 26.5	-05 15 05	14.909 ± 0.019	14.174 ± 0.018	M5.5 ^g
1213_413	05 35 06.9	-05 11 50	16.702 ± 0.043	15.601 ± 0.030	14.928 ± 0.024	M4-M4.5 ^g	0.7	...
CHS 8782	05 35 16.2	-05 15 48	17.157 ± 0.013	16.448 ± 0.023	14.935 ± 0.011	14.262 ± 0.011	13.869 ± 0.014	M5.25 ^h	0.1	...

^aCoordinates from 2MASS final release.

^bMagnitudes and relative uncertainties from 4-Shooter photometry.

^cMagnitudes and relative uncertainties from SQUID photometry.

^dKeck LRIS spectra.

^eBlue Channel MMT spectra.

^fRed Channel MMT spectra.

^gSpeX IRTF spectra.

^hCorMASS spectra.

iA_H values calculated from $J - H$ colors (see Appendix A) and not from the A_V values found as the best fit from spectral classification.

Table 4. Summary of Spectral Observations: Field Stars and Objects of Indeterminate Type

Name ...	R. A. ^a (J2000)	Dec. ^a (J2000)	I, σ_I^b (mag)	$z', \sigma_{z'}^b$ (mag)	J, σ_J^c (mag)	H, σ_H^c (mag)	K, σ_K^c (mag)	Sp. Type ...	A_H^i ...
6	05 35 15.5	-05 08 59	17.332 ± 0.010	16.722 ± 0.022	15.716 ± 0.013	15.078 ± 0.013	14.841 ± 0.015	M3.25V ^d	0.1
12	05 34 54.9	-05 02 43	19.555 ± 0.042	18.293 ± 0.052	17.084 ± 0.029	16.052 ± 0.019	15.631 ± 0.021	... ^f	0.6
16	05 35 09.0	-05 10 26	15.938 ± 0.003	15.579 ± 0.005	14.602 ± 0.008	13.926 ± 0.008	13.711 ± 0.010	M2.5V ^e	0.1
25	05 35 07.8	-05 01 19	19.655 ± 0.070	18.316 ± 0.055	16.254 ± 0.018	15.463 ± 0.016	15.003 ± 0.016	M8IV ^{f,k}	0.3
01	05 34 46.8	-05 04 27	19.837 ± 0.062	18.247 ± 0.046	16.910 ± 0.027	15.849 ± 0.018	15.335 ± 0.019	M4V ^f	0.7
74	05 34 58.2	-05 07 13	20.022 ± 0.111	18.542 ± 0.072	16.868 ± 0.023	15.729 ± 0.017	15.213 ± 0.017	M3V ^f	0.8
79	05 34 43.5	-05 14 21	17.544 ± 0.024	17.035 ± 0.023	15.300 ± 0.014	14.287 ± 0.009	13.976 ± 0.010	K? ^f	0.6
558_371	05 35 31.4	-05 12 00	14.558 ± 0.010	13.962 ± 0.011	13.656 ± 0.013	M5V ^g	0.0
650_963	05 35 27.3	-05 05 27	17.220 ± 0.034	16.340 ± 0.023	15.601 ± 0.028	... ^g	0.4
820_1131	05 35 19.7	-05 03 35	16.705 ± 0.034	15.270 ± 0.017	... ^g	...
513_395	05 35 33.4	-05 11 45	16.899 ± 0.070	16.012 ± 0.073	14.909 ± 0.053	... ^g	0.4
1107_414	05 35 06.9	-05 11 33	17.877 ± 0.050	16.136 ± 0.028	15.145 ± 0.021	... ^g	1.6
652_1582	05 35 27.2	-04 58 35	17.215 ± 0.057	15.571 ± 0.027	... ^g	...
1164_263	05 35 04.3	-05 13 13	17.380 ± 0.047	16.251 ± 0.031	15.317 ± 0.027	... ^g	0.7
455_461	05 35 36.0	-05 11 01	16.854 ± 0.063	15.692 ± 0.048	... ^g	...
995_1280	05 35 11.9	-05 01 56	17.865 ± 0.042	16.292 ± 0.024	15.263 ± 0.017	... ^g	1.4
1095_766	05 35 07.4	-05 07 38	17.661 ± 0.039	15.730 ± 0.017	14.665 ± 0.013	... ^g	1.9
1068_598	05 35 08.6	-05 09 30	17.117 ± 0.034	15.550 ± 0.016	14.728 ± 0.013	... ^g	1.4
925_1442	05 35 15.0	-05 00 08	16.350 ± 0.052	14.827 ± 0.023	... ^g	...
657_1084	05 35 27.0	-05 04 07	14.077 ± 0.033	... ^g	...
814_1360	05 35 20.0	-05 01 03	14.325 ± 0.019	... ^g	...
643_957	05 35 27.6	-05 05 31	14.870 ± 0.024	... ^g	...
706_829	05 35 24.8	-05 06 56	13.897 ± 0.009	... ^g	...
356_225	05 35 45.1	-05 13 56	18.086 ± 0.066	17.684 ± 0.071	16.479 ± 0.030	15.397 ± 0.026	14.776 ± 0.029	M4V ^g	0.7
1191_569	05 35 07.9	-05 10 06	16.922 ± 0.026	15.534 ± 0.016	14.893 ± 0.014	... ^g	1.1
1163_564	05 35 09.1	-05 10 09	16.993 ± 0.040	15.699 ± 0.019	14.995 ± 0.019	... ^g	1.0
469_431	05 35 40.0	-05 11 38	18.377 ± 0.071	17.913 ± 0.088	16.568 ± 0.029	15.473 ± 0.023	14.830 ± 0.019	... ^g	0.7
1448_85	05 34 56.4	-05 15 28	17.357 ± 0.055	15.817 ± 0.027	14.915 ± 0.029	... ^g	1.3
391_684	05 35 43.5	-05 08 50	18.052 ± 0.056	17.801 ± 0.036	15.790 ± 0.016	14.777 ± 0.011	14.091 ± 0.010	... ^g	0.6
708_1277	05 35 29.4	-05 02 15	17.118 ± 0.025	15.490 ± 0.014	14.710 ± 0.014	... ^g	1.4
1821_1428	05 34 39.8	-05 00 34	18.822 ± 0.027	18.317 ± 0.043	16.723 ± 0.027	15.508 ± 0.019	14.813 ± 0.018	... ^g	0.9
1350_447	05 35 00.8	-05 11 27	16.772 ± 0.026	15.193 ± 0.014	14.440 ± 0.012	... ^g	1.4
1137_1202	05 35 10.3	-05 03 05	17.001 ± 0.032	15.128 ± 0.013	14.183 ± 0.010	... ^g	1.8

Table 4—Continued

Name ...	R. A. ^a (J2000)	Dec. ^a (J2000)	I, σ_I ^b (mag)	z' , $\sigma_{z'}$ ^b (mag)	J, σ_J ^c (mag)	H, σ_H ^c (mag)	K, σ_K ^c (mag)	Sp. Type ...	A_H ⁱ ...
558_282	05 35 36.1	-05 13 17	16.714 ± 0.060	15.027 ± 0.029	14.217 ± 0.031	... g	1.5
554_173	05 35 36.3	-05 14 30	14.455 ± 0.014	13.818 ± 0.013	... g	...
1442_484	05 34 56.7	-05 11 03	17.141 ± 0.032	15.657 ± 0.021	14.941 ± 0.017	... g	1.2
1526_99	05 34 53.0	-05 15 19	16.288 ± 0.022	15.000 ± 0.014	14.404 ± 0.014	... g	1.0
164_563(a,b) ^j	05 35 53.6	-05 10 10	18.081 ± 0.028	17.667 ± 0.040	16.185 ± 0.018	15.237 ± 0.015	14.681 ± 0.015	... g	0.5
458_1202b	05 35 40.5	-05 03 05	19.173 ± 0.044	18.615 ± 0.043	16.610 ± 0.038	15.278 ± 0.016	14.706 ± 0.016	... g	1.0
458_1202a	05 35 40.3	-05 03 06	19.308 ± 0.031	18.721 ± 0.044	17.194 ± 0.054	15.783 ± 0.028	15.290 ± 0.030	... g	1.1
269_588	05 35 48.9	-05 09 53	19.078 ± 0.032	17.509 ± 0.075	16.243 ± 0.018	15.069 ± 0.013	14.513 ± 0.016	... g	0.8
781_708	05 35 26.2	-05 08 34	15.490 ± 0.026	15.200 ± 0.027	14.607 ± 0.023	... g	0.0
301_833	05 35 47.5	-05 07 10	18.363 ± 0.067	...	16.308 ± 0.020	15.212 ± 0.013	14.672 ± 0.013	... g	0.7
1224_1205	05 35 06.4	-05 03 03	19.527 ± 0.033	18.321 ± 0.024	16.191 ± 0.016	14.859 ± 0.011	14.289 ± 0.011	... g	1.0
1512_410	05 34 53.6	-05 11 52	19.043 ± 0.040	17.962 ± 0.040	15.698 ± 0.013	14.480 ± 0.010	13.897 ± 0.009	... g	0.9
583_352	05 35 35.0	-05 12 31	16.405 ± 0.062	15.473 ± 0.057	14.568 ± 0.095	... h	0.5
d216-0939	05 35 21.6	-05 09 39	13.879 ± 0.006	12.918 ± 0.005	12.222 ± 0.004	< M3 ^h	0.5
CHS 9695	05 35 22.4	-05 07 39	14.741 ± 0.014	12.087 ± 0.004	10.268 ± 0.002	\lesssim M3 ^h	2.9

^aCoordinates from 2MASS final release.

^bMagnitudes and relative uncertainties from 4-Shooter photometry.

^cMagnitudes and relative uncertainties from SQUIID photometry.

^dKeck LRIS spectra.

^eBlue Channel MMT spectra.

^fRed Channel MMT spectra.

^gSpeX IRTF spectra.

^hCorMASS spectra.

ⁱ A_H values calculated from $J - H$ colors (see Appendix A) and not from the A_V values found as the best fit from spectral classification.

^jSource is unresolved in imaging but was resolved on the slit.

^kThis source has a spectral type later than M6.5 and is a young brown dwarf in OMC 2/3. However, it serendipitously fell into the slit during the observation and although we have reconstructed which source it is, and believe it is the one whose coordinates and magnitudes are listed here, until we are confident this is the correct source, we have chosen to put it in this table. It is also an accreting brown dwarf; it has an $\text{EW}[\text{H}\alpha] < -40$.

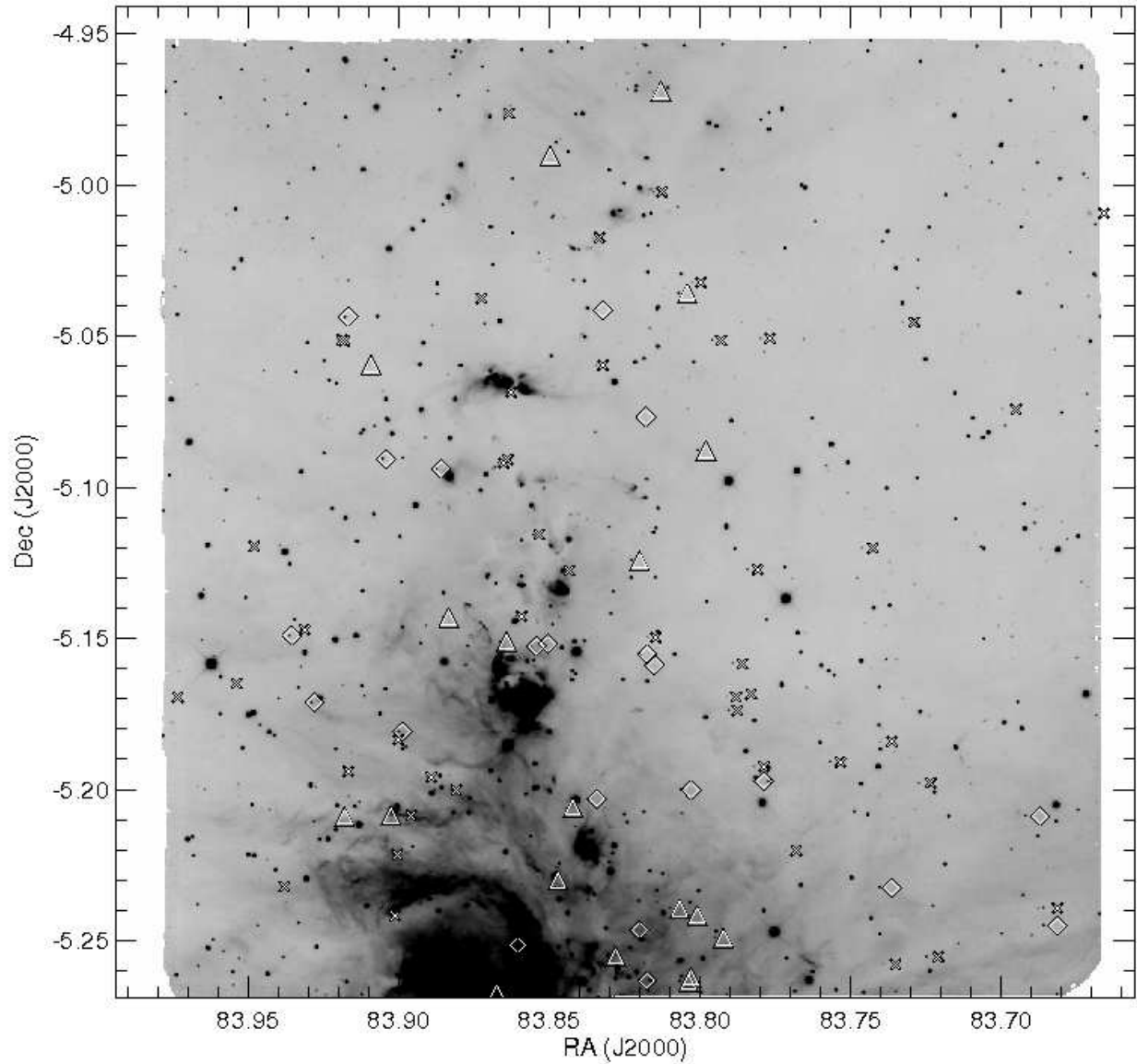


Fig. 1.— An inverse-scale SQIID image of OMC 2/3 in the K -band. The distribution of the 40 low new low mass members is shown: the 19 sources with spectral types of M6.5–M9 from Table 2 (triangles), and the 21 sources with spectral types of M4–M6 from Table 3 (diamonds). For reference, we also show the sources from Table 4 (crosses) which are field stars or whose spectral types we were unable to determine.

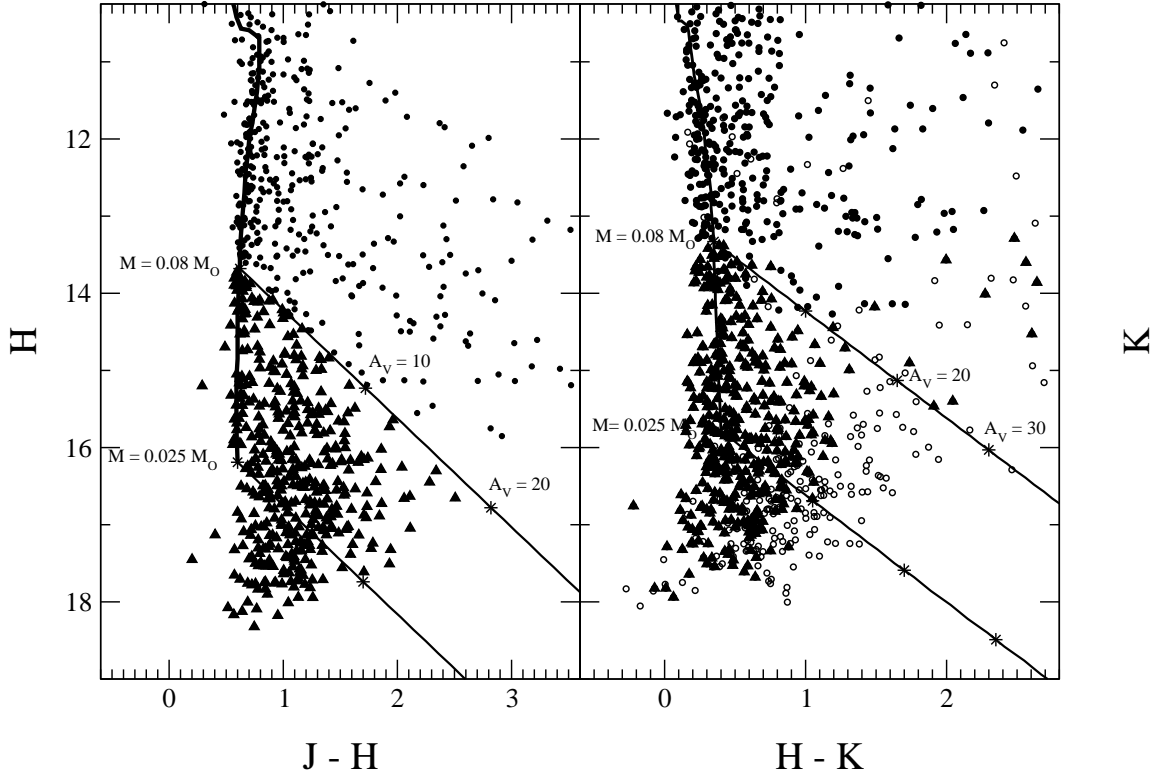


Fig. 2.— These two color-magnitude diagrams show all sources detected at J -, H - and K -band in the SQUID image with photometric uncertainties less than 0.15 magnitudes (filled circles). The H versus $J - H$ CMD on the left identifies, as filled triangles, the brown dwarf candidates selected based on their location near or below the HBL. Over-plotted is the 1 Myr Baraffe et al. (1998) evolutionary isochrone, assuming a distance to OMC 2/3 of 450 pc. In addition, reddening vectors (Cohen et al. 1981) are plotted for a $0.08 M_{\odot}$ source with an age of 1 Myr (upper diagonal line) and a $25 M_{Jup}$ brown dwarf with an age of 1 Myr (lower diagonal line). The plot on the right shows, with the same symbols, the brown dwarf candidates on a K versus $H - K$ CMD. Many of the red sources near the HBL on the H versus $J - H$ CMD are above the HBL on the K versus $H - K$ CMD; these sources may have strong infrared excesses. The open circles represent sources detected in the H and K -bands (and not in J).

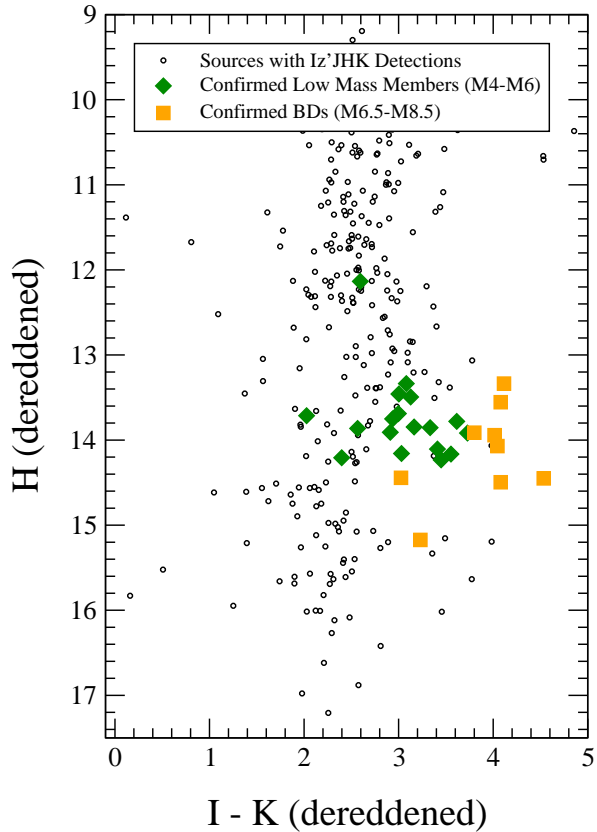


Fig. 3.— Dereddened color-magnitude diagram for OMC 2/3 assuming an intrinsic $J - H$ color of a late M star for each source (see Appendix A). The positions of known brown dwarfs define the region of the color-magnitude plane populated by young brown dwarfs at the distance of Orion. We find that the spectroscopically verified brown dwarfs in OMC 2/3 (filled squares; colored orange in electronic edition) occupy a very limited region of the color-magnitude plane. See the electronic edition of the Journal for a color version of this figure.

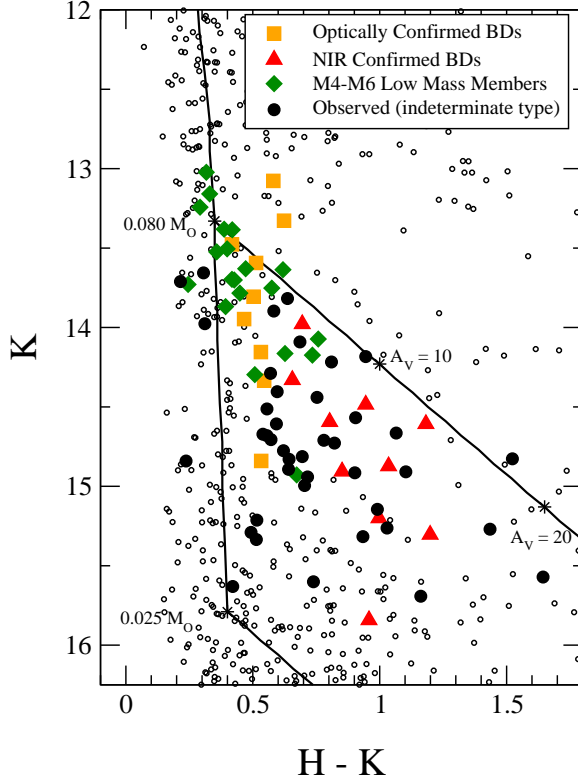


Fig. 4.— K vs. $H - K$ color-magnitude diagram showing all 1017 sources detected at H and K with uncertainties less than 0.15 magnitudes in OMC 2/3 (open black circles). Overplotted is the Baraffe et al. (1998) evolutionary isochrone for a 1 Myr-old pre-main sequence star, assuming a distance to OMC 2/3 of 450 pc. Reddening vectors are plotted for: 1) a $0.08 M_{\odot}$ star (upper diagonal line) and 2) a $25 M_J$ brown dwarf with an age of 1 Myr (lower diagonal line). Brown dwarfs confirmed by far-red and near-infrared spectroscopy are denoted by filled squares (colored orange in electronic edition) and triangles (colored red in electronic edition), respectively. Sources denoted by filled diamonds (colored green in electronic edition) are the 21 candidates confirmed by spectroscopy to be M4–M6 low mass members. Sources denoted by filled circles were observed with SpeX during the December 2003, January 2005 and 2006 runs; they exhibit featureless spectra, which we argue makes them likely background sources with spectral types earlier than M4. Note that some brown dwarfs were found with magnitudes above the HBL. These may be due to ages younger than the assumed 1 Myr age and/or the presence of infrared excess. See the electronic edition of the Journal for a color version of this figure.

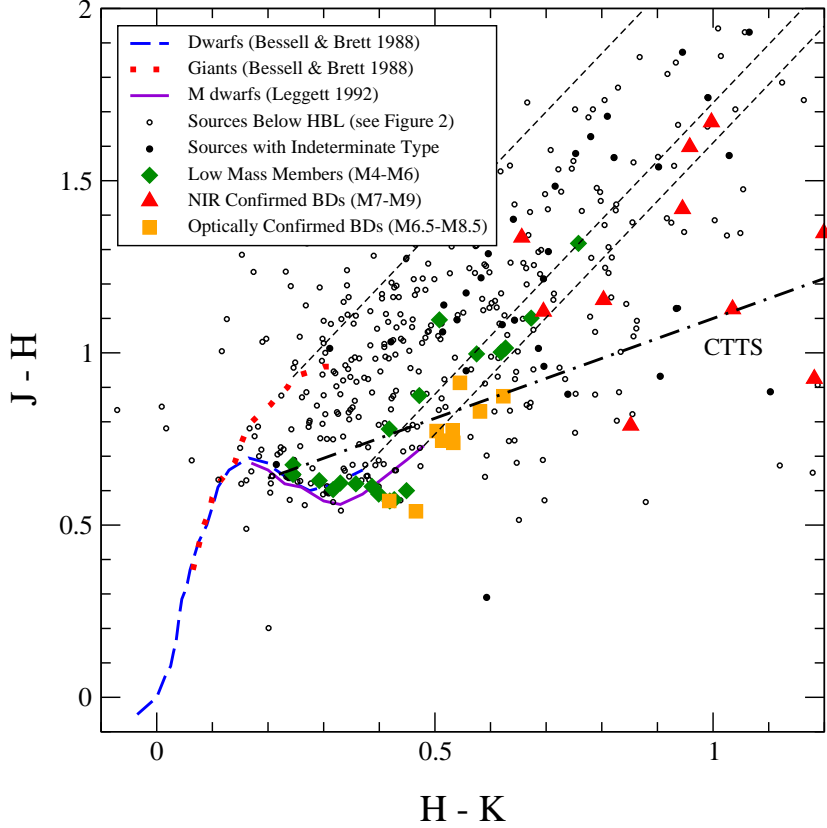


Fig. 5.— The above $J - H$ versus $H - K$ color-color diagram for OMC 2/3 shows SQUIID photometry for the brown dwarf candidates: the sources with color magnitude errors less than 0.15 magnitudes that appear below the $0.08 M_{\odot}$ reddening line in the H versus $J - H$ CMD (see Figure 2). Those sources that are either field stars or whose spectral types could not be determined (see Table 4) are shown as filled circles. The sources spectroscopically confirmed as M4–M9 members are compared with, from Bessell & Brett (1988), the colors of giants (dotted locus colored red in electronic edition) and dwarfs (dashed locus colored blue in electronic edition), as well as M dwarfs from Leggett (1992, solid line colored purple in electronic edition). (Note that these colors have not been transformed into the SQUIID photometric system.) Small dashed lines indicate reddening vectors (Cohen et al. 1981) for (from left) M5 giants, M6 dwarfs, and M9 sources (typical colors for M9 stars from Kirkpatrick et al. (2000)). The dot-dashed line is the classical T Tauri star locus from Meyer, Calvet, & Hillenbrand (1997) in Taurus. See the electronic edition of the Journal for a color version of this figure.

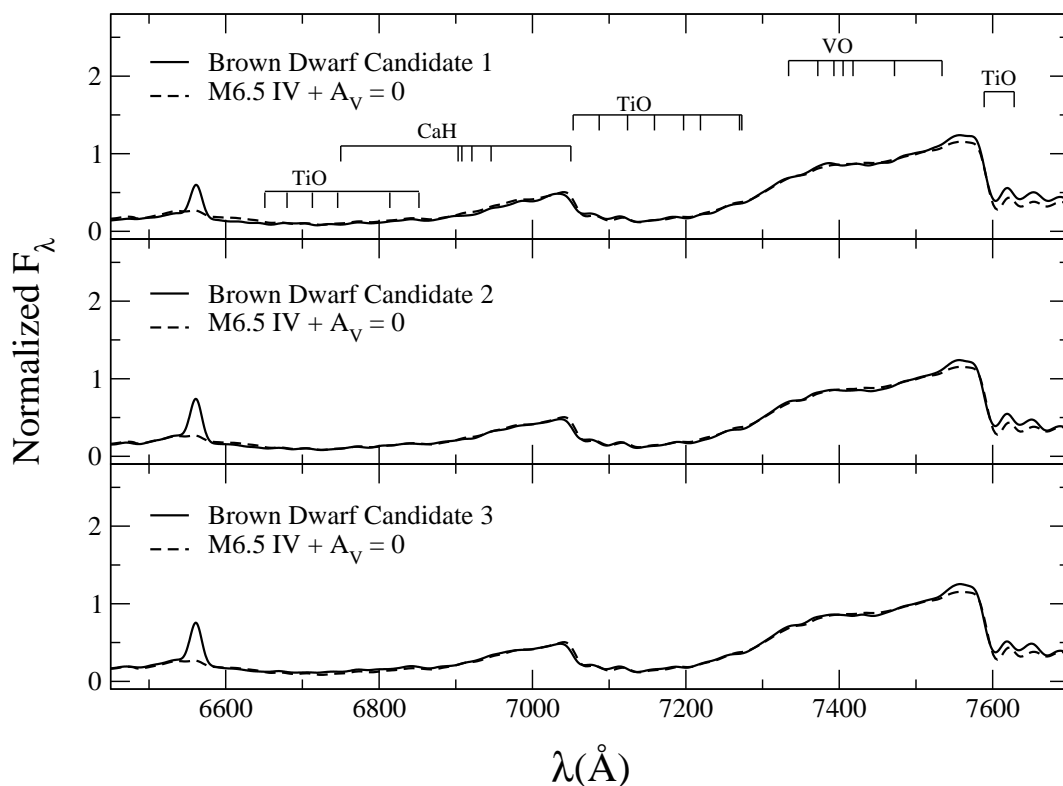


Fig. 6.— Candidate brown dwarf spectra obtained with LRIS on Keck I. The over-plotted dotted lines show the reference spectra used to classify the candidates. All three of these candidates look very similar: each has an M6.5 spectral type with little or no reddening and all exhibit H α (at 6563 \AA). In addition, they all match the average spectrum of a M6.5 dwarf and giant: indicating a young source. The TiO, CaH and VO molecular bands in this wavelength range used for spectral classification are indicated. Each of the spectra have been smoothed to a resolution of 18 \AA and normalized at 7500 \AA .

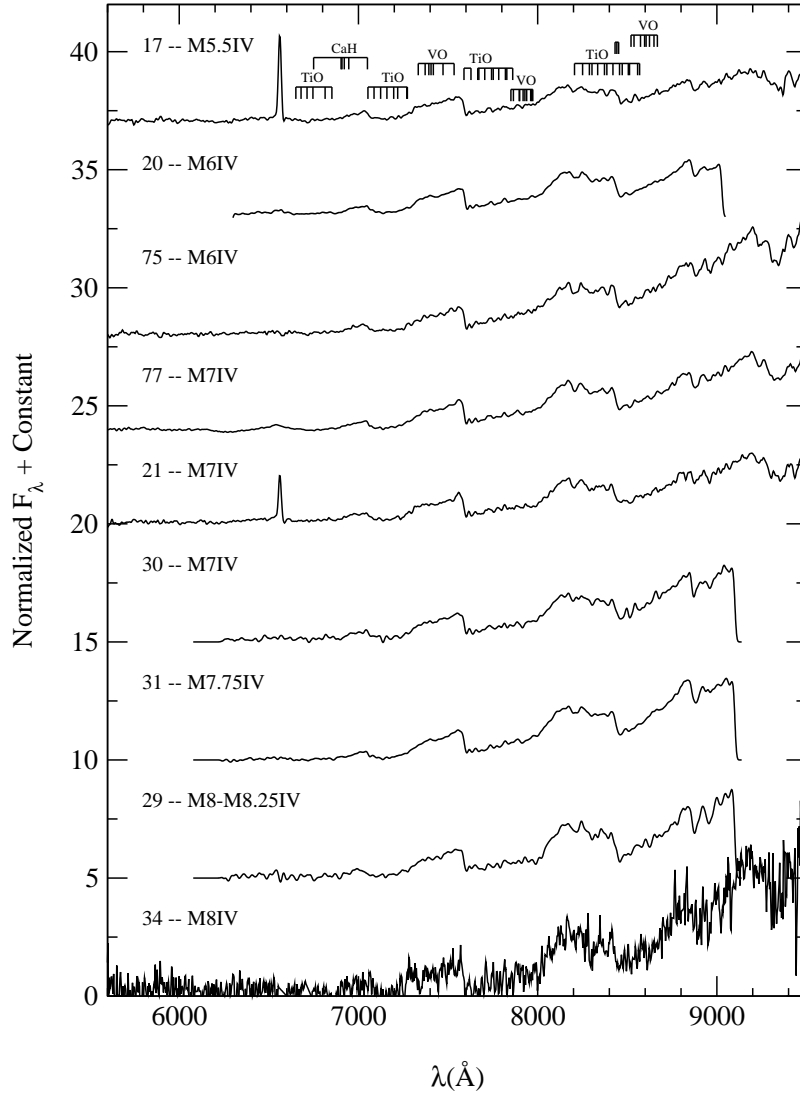


Fig. 7.— Low resolution spectra from the MMT with the Red (5500–9800 Å) and Blue (6200–9000 Å) Channel Spectrographs of nine new low mass members in OMC 2/3. The TiO, CaH, and VO molecular bands used for spectral classification are indicated. Strong H α emission can be seen in two of the sources: 17 and 21. The spectra have been smoothed to a resolution of 18 Å and normalized at 7500 Å.

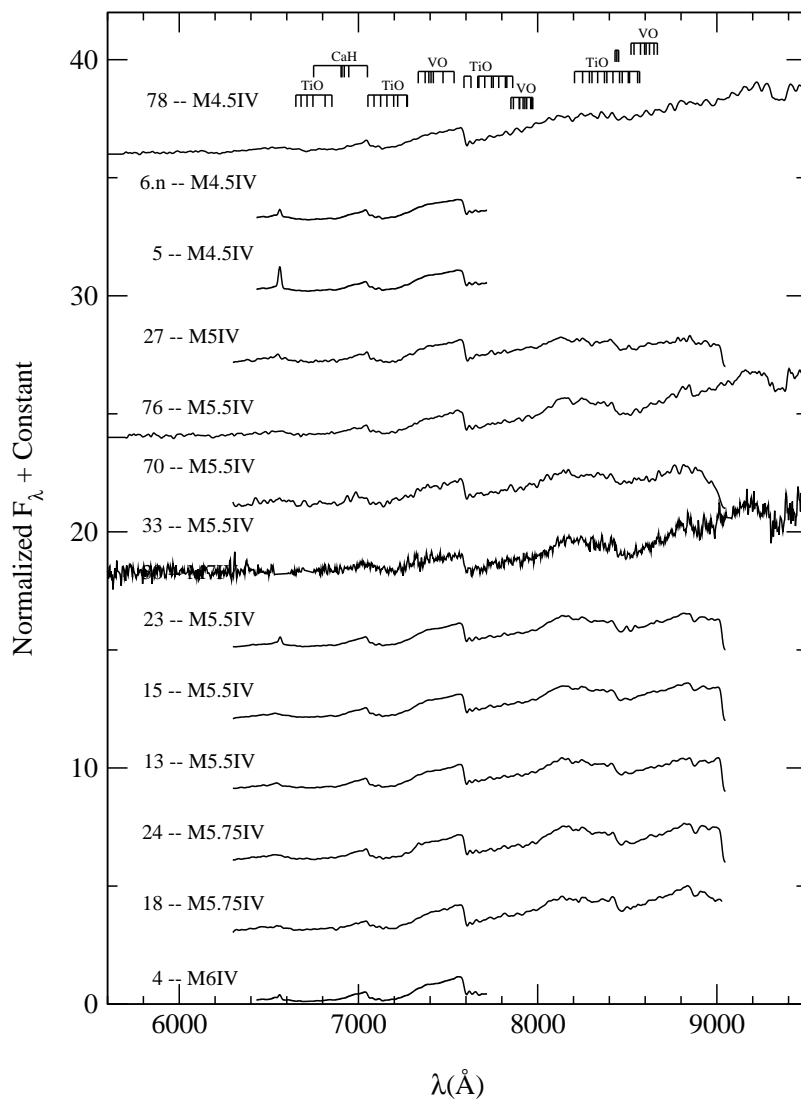


Fig. 8.— Low resolution spectra obtained with LRIS (6400–7700 \AA) on Keck I as well as with the Red (5500–9800 \AA) and Blue (6200–9000 \AA) Channel Spectrographs on the MMT of thirteen new low mass members in OMC 2/3. The TiO, CaH, and VO molecular bands used for spectral classification are indicated. The spectra have been smoothed to a resolution of 18 \AA and normalized at 7500 \AA .

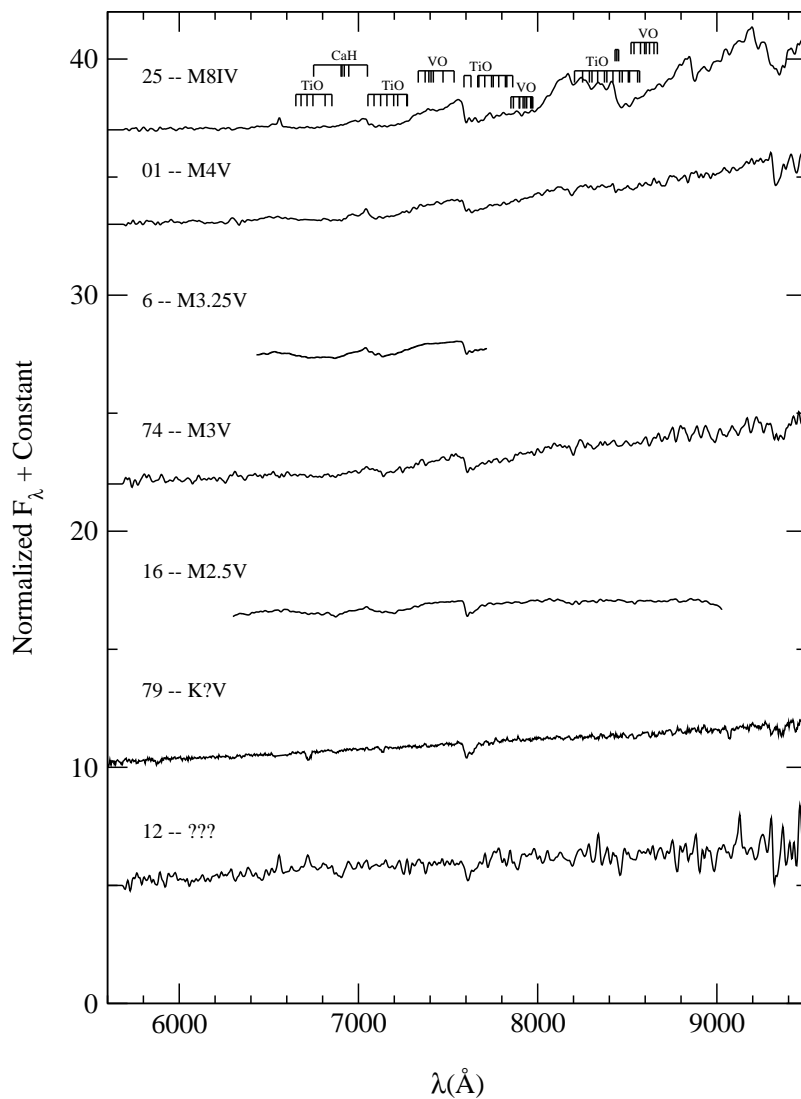


Fig. 9.— Low resolution spectra obtained with LRIS (6400–7700 Å) on Keck I as well as with the Red (5500–9800 Å) and Blue (6200–9000 Å) Channel Spectrographs on the MMT of candidate brown dwarfs in OMC 2/3 that are either field dwarfs, or whose spectral types are undetermined (from Table 4). Note that candidate 25 is indeed a young brown dwarf, and has been classified as such; however, this source was serendipitously observed and since we are not confident we have the correct source due to uncertainties in reconstructing its position, it is grouped with the unclassified sources. The spectra have been smoothed to a resolution of 18 Å and normalized at 7500 Å.

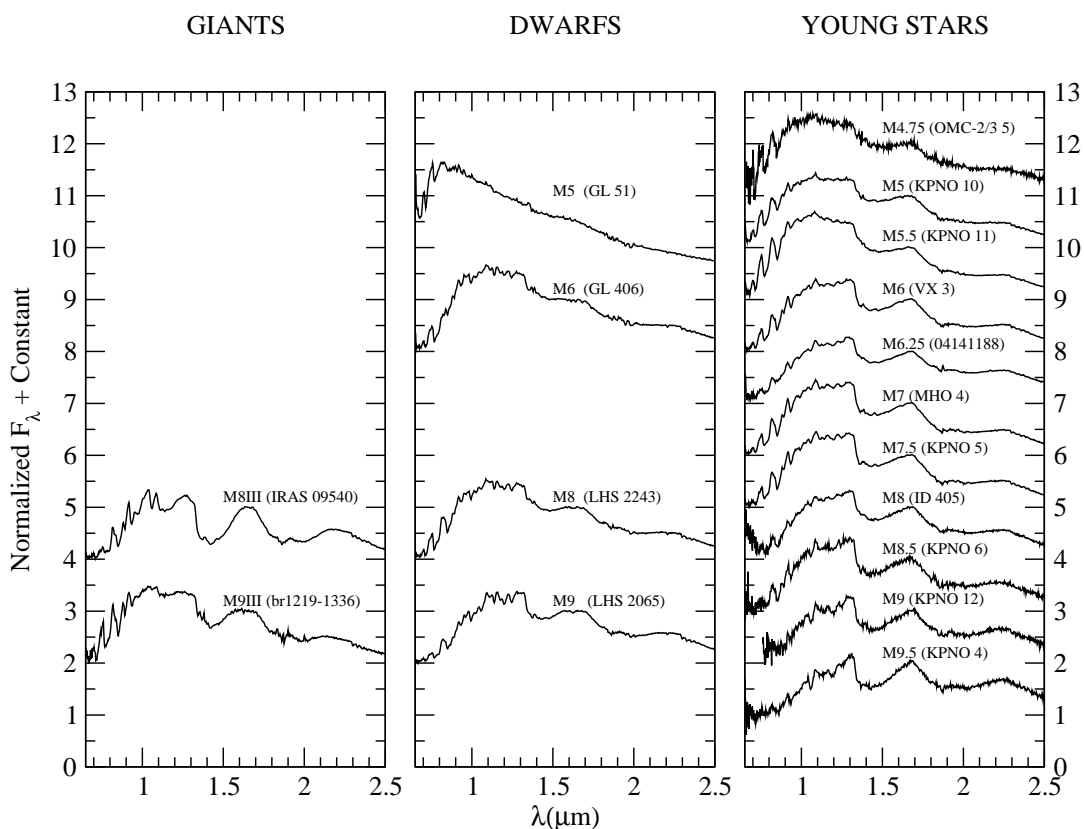


Fig. 10.— For comparison with the OMC 2/3 brown dwarf candidate near-infrared spectra, a grid of standards was also obtained with the SpeX Spectrograph in single-prism mode ($\lambda/\Delta\lambda \sim 250$). These objects were classified from their far-red spectra in Briceño et al. (2002) and Luhman et al. (2003). A representative sample of the SpeX spectra of these standards is presented here. They were observed during the December 2003 run described in Section 4.2.1 as well as by Luhman (2006) and Muench et al. (2007). These spectra have all been normalized at a wavelength of $1.66 \mu\text{m}$.

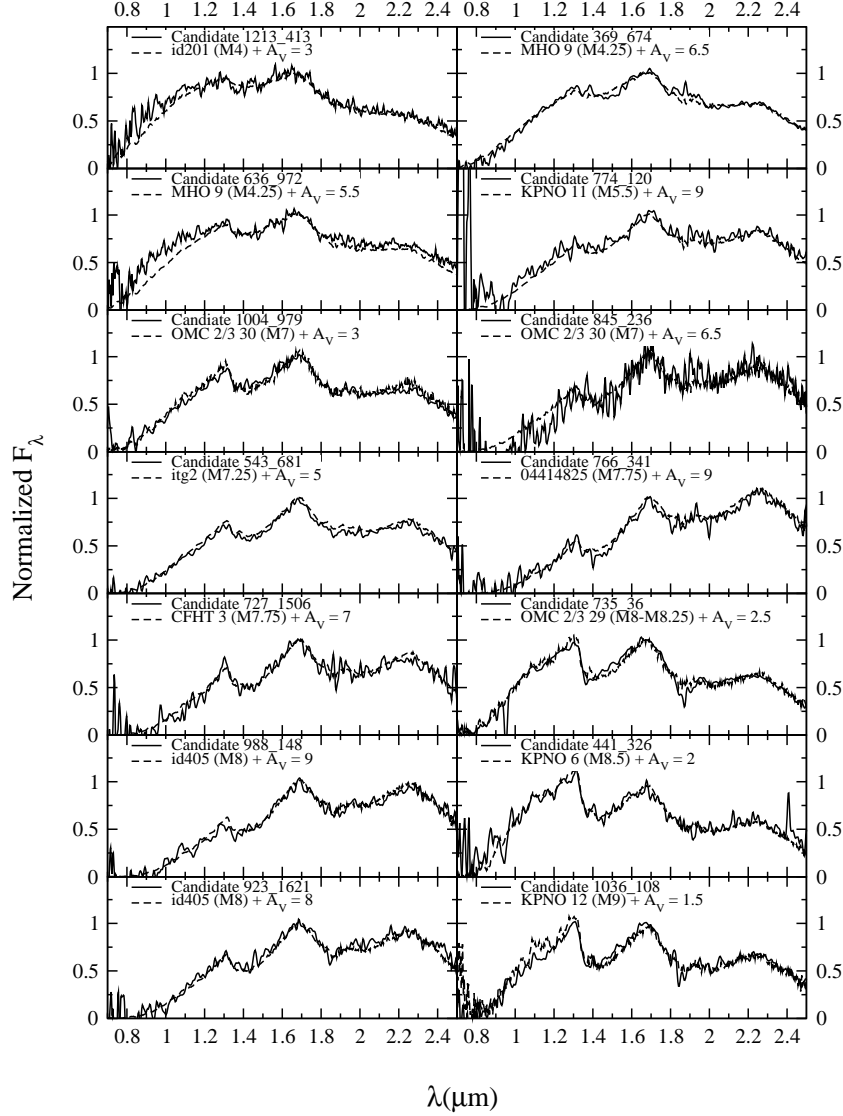


Fig. 11.— These 14 spectra of embedded OMC 2/3 members (solid lines) were obtained at the IRTF with SpeX in single-prism mode ($\lambda/\Delta\lambda \sim 250$); for display purposes they have been smoothed with a Gaussian kernel. The reddened reference spectra (dashed lines) with the best match to the candidates are over-plotted. The reference spectra were also observed with SpeX, but their spectral types were obtained from far-red spectra. Note the locations of the H₂O and CO absorption bands, the shapes of which were used for spectral classification. All spectra were normalized at a wavelength of 1.68 μm .

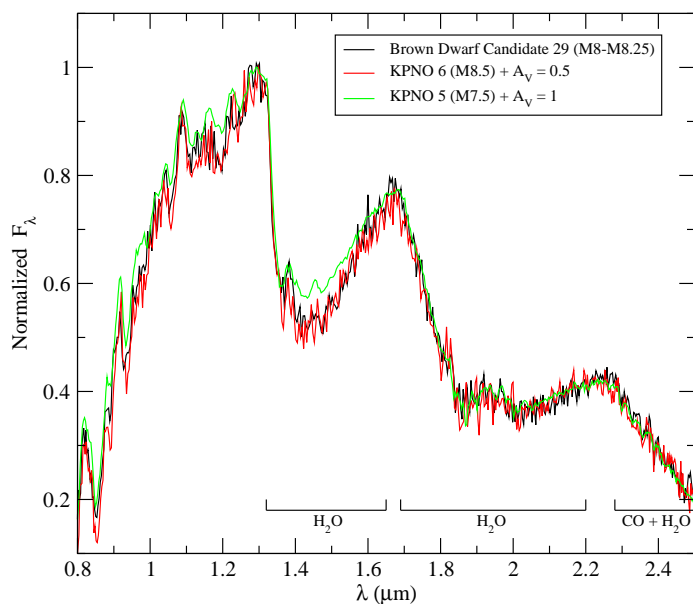


Fig. 12.— The spectrum of brown dwarf candidate 29 (solid line) obtained at the IRTF with the SpeX Spectrograph in single-prism mode ($\lambda/\Delta\lambda \sim 250$). This brown dwarf was classified from its far-red spectrum (see Figure 7) as M8–M8.25 with $A_V = 0$. The dashed line (colored red in electronic edition) shows the SpeX reference spectrum from a young member in Taurus, KPNO 6, with a spectral type of M8.5 and given a reddening of $A_V=0.5$, which yields a spectrum very similar to OMC 2/3 brown dwarf candidate 29. The spectrum from KPNO 5 (dotted line colored green in electronic edition), a Taurus low mass member with a known spectral type of M7.5 (Briceño et al. 2002) is also shown; note that the OMC 2/3 brown dwarf candidate spectrum is a better match to the M8.5 spectrum than the M7.5 spectrum (specifically when looking at the depth of the steam band from 1.3–1.5 μm). An uncertainty of ± 0.5 subclass is typical for these spectra. All three spectra were normalized at a wavelength of 1.30 μm . See the electronic edition of the Journal for a color version of this figure.

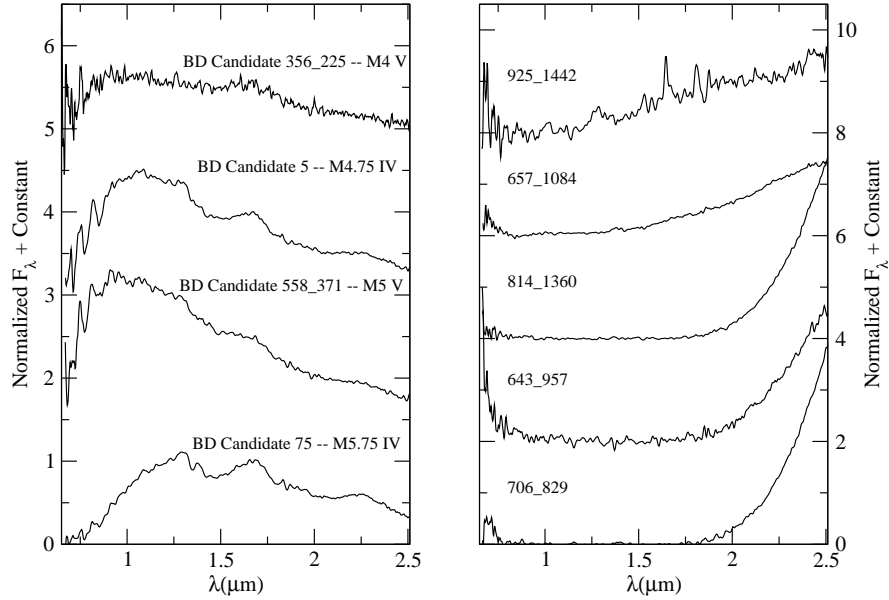


Fig. 13.— These 9 spectra were obtained at the IRTF with SpeX in single-prism mode ($\lambda/\Delta\lambda \sim 250$); for display purposes they have been smoothed with a Gaussian kernel. In the left-hand panel, we show the spectra that have been classified as either members (IV spectral class) or dwarfs (V spectral class). Brown dwarf candidates 5 and 75 are young stars which have already been displayed in the far-red in Figures 8 and 7, respectively. The sources in the right-hand panel all had indeterminate spectral types (Table 4). The spectra in the left-hand panel were normalized at a wavelength of $1.68 \mu\text{m}$, and in the right-hand panel, they were normalized at a wavelength of $2.2 \mu\text{m}$. The photometry for these sources appears in Tables 3 and 4.

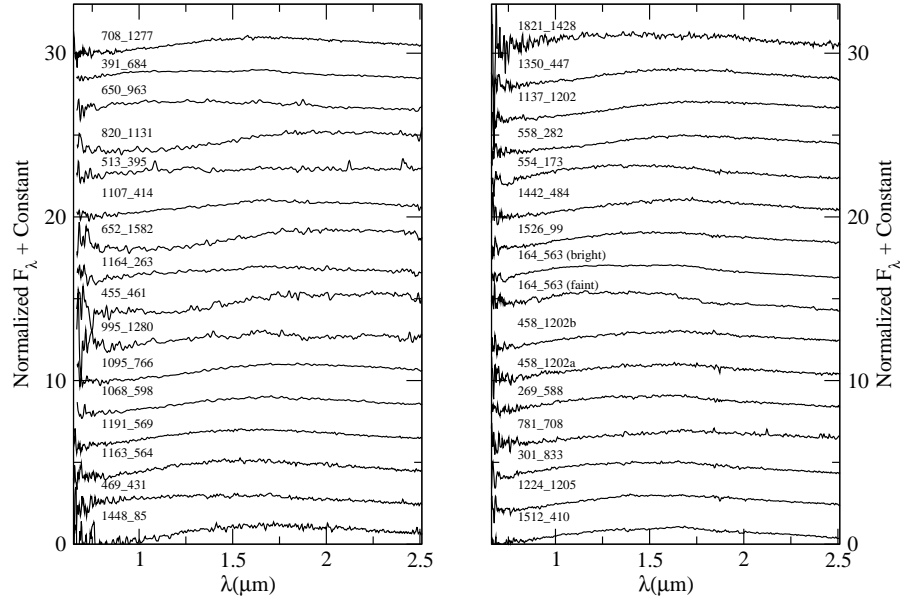


Fig. 14.— These 32 spectra, all sources with indeterminate spectral types (Table 4), were obtained at the IRTF with SpeX in single-prism mode ($\lambda/\Delta\lambda \sim 250$); for display purposes they have been smoothed with a Gaussian kernel. The photometry for these sources appears in Table 4. All spectra were normalized at a wavelength of $1.68 \mu\text{m}$.

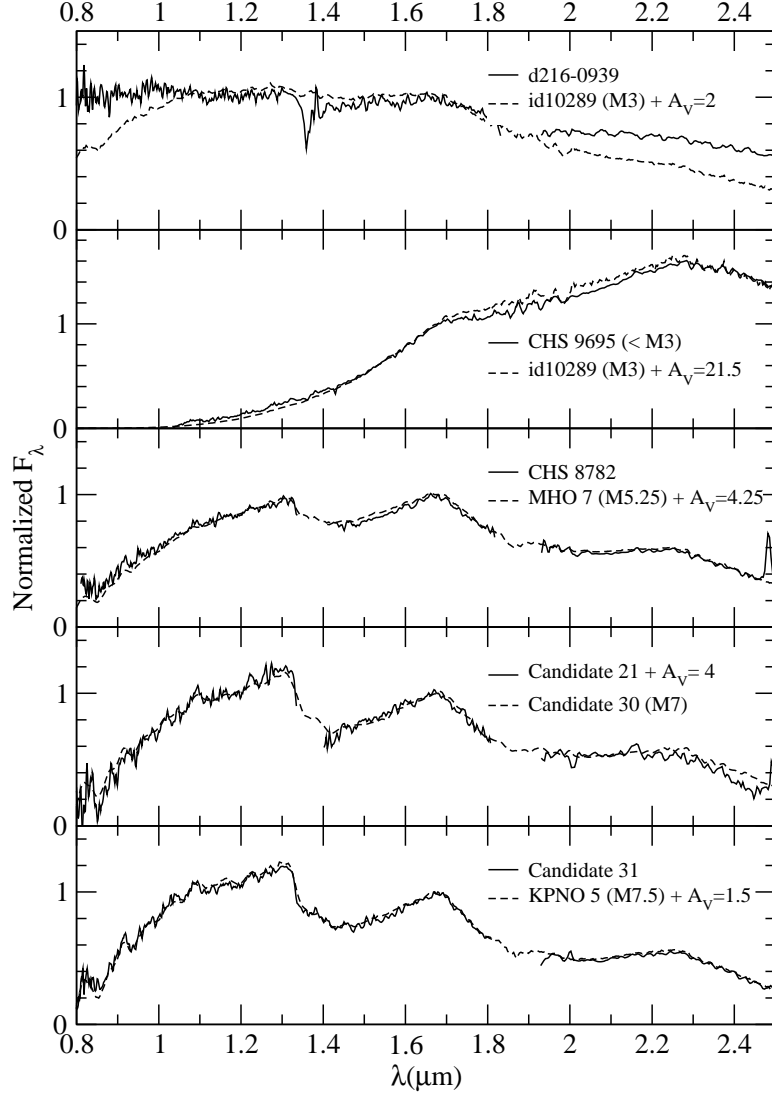


Fig. 15.— These 5 spectra (solid lines) were obtained with CorMASS ($\lambda/\Delta\lambda \sim 300$); for display purposes they have been smoothed with a Gaussian kernel and some regions where telluric was very noisy have been removed. Reference spectra obtained with SpeX (dashed lines) with the best match to the candidates are over-plotted (spectral types determined from far-red spectra). Note that candidate 21 (obtained with CorMASS) is virtually identical to candidate 30 (obtained with SpeX); both candidates were classified as M7 from far-red spectra. All spectra have been normalized at $1.68 \mu\text{m}$.

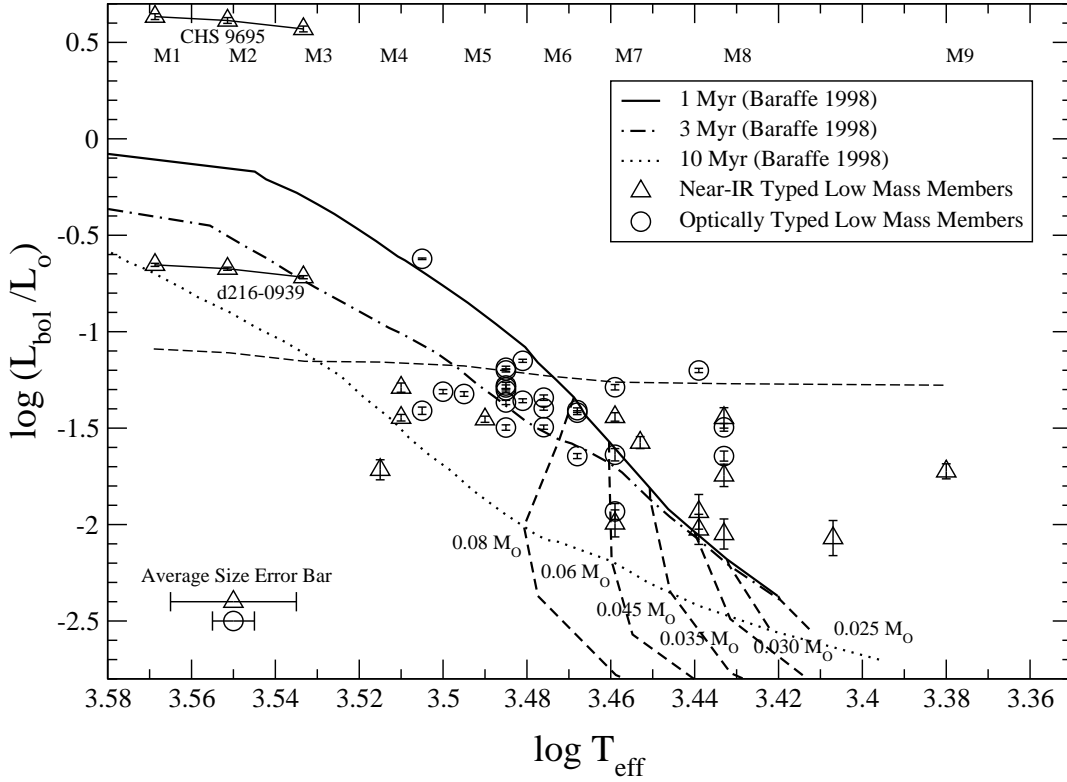


Fig. 16.— A $\log(L_{bol}/L_{\odot})$ versus $\log T_{eff}$ H-R diagram for the spectroscopically confirmed low mass members of OMC 2/3. Open circles indicate those whose spectral types were determined from far-red spectra and open triangles indicate those determined using near-infrared spectra. Baraffe et al. (1998) evolutionary isochrones are shown for a 1 (top solid black line), 3 (middle dot-dashed line), and 10 (bottom dotted line) Myr-old PMS star. The dashed lines indicate lines of constant mass, from left to right, 0.08 M_{\odot} , 0.06 M_{\odot} , 0.045 M_{\odot} , 0.035 M_{\odot} , 0.030 M_{\odot} and 0.025 M_{\odot} . The upper luminosity limit used to select the brown dwarf candidates is over-plotted (dashed line) to show the selection effect. Two candidates observed with CorMASS, CHS 9695 and d216-0939 (the edge-on disk) are added here with their upper spectral classification limit of M3 to show where they appear on the diagram as an M1, M2 or M3 source. Average error bars for uncertainty in $\log T_{eff}$ are shown in the lower left-hand corner (± 0.5 subclass uncertainty in spectral type for the NIR classified sources, and ± 0.25 subclass uncertainty for the optically classified sources). The error bars shown for the $\log(L_{bol}/L_{\odot})$ axis are based on photometric uncertainties from the $J - H$ colors.

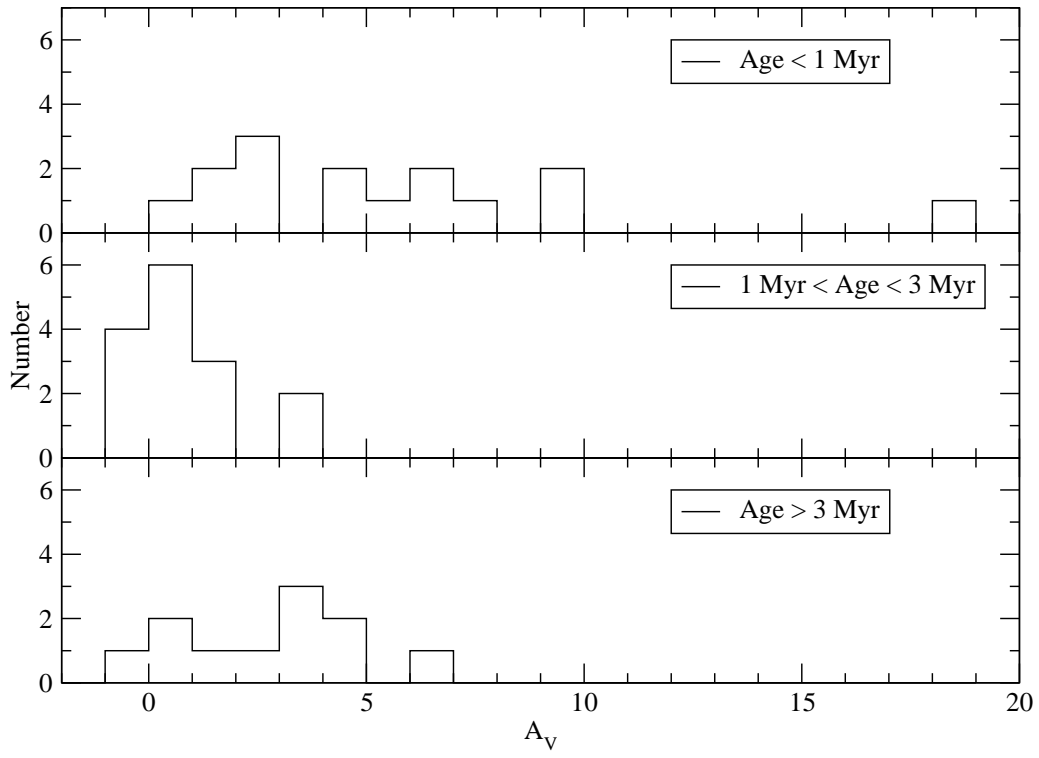


Fig. 17.— Comparison of the values of A_V for sources in three different age groupings: less than 1 Myr, between 1 and 3 Myr and greater than 3 Myr.